

Review

# Water-in-Salt Electrolytes: Advances and Chemistry for Sustainable Aqueous Monovalent-Metal-Ion Batteries

Rashmi Nidhi Mishra , Anil Kumar Madikere Raghunatha Reddy , Marc-Antoni Goulet \* and Karim Zaghib \*

Department of Chemical and Materials Engineering, Concordia University, 1455 De Maisonneuve Blvd. West, Montreal, QC H3G 1M8, Canada; rashmi.nidhi@mail.concordia.ca (R.N.M.); anil.mr@concordia.ca (A.K.M.R.R.)

\* Correspondence: marcanton.goulet@concordia.ca (M.-A.G.); karim.zaghib@concordia.ca (K.Z.)

**Abstract:** Electrolytes play a vital role in the performance and safety of electrochemical energy storage devices, such as lithium-ion batteries (LIBs). While traditional LIBs rely on organic electrolytes, these flammable solutions pose safety risks and require expensive, moisture-sensitive manufacturing processes. Aqueous electrolytes offer a safer, more cost-effective alternative, but their narrow electrochemical window, corrosivity to electrodes, and enabling of dendritic growth on metal anodes limit their practical applications. Water-in-salt electrolytes (WiSEs) have emerged as a promising solution to these challenges. By significantly reducing water activity and forming a stable solid–electrolyte interphase (SEI), WiSEs can expand the electrochemical stability window, inhibit material dissolution, and suppress dendritic growth. This unique SEI formation mechanism, which is similar to that observed in organic electrolytes, contributes to the improved performance and stability of WiSE-based batteries. Additionally, the altered solvation structure of WiSEs minimizes the presence of free water molecules, further stabilizing the SEI and reducing water activity. This review comprehensively examines the composition, mechanisms, and characterization of WiSEs and their application in monovalent-metal-ion batteries.

**Keywords:** water-in-salt electrolytes; metal-ion batteries; sodium-ion batteries; lithium-ion batteries; potassium-ion batteries; monovalent-metal-ion batteries



Received: 24 February 2025

Revised: 14 March 2025

Accepted: 21 March 2025

Published: 22 March 2025

**Citation:** Mishra, R.N.; Madikere Raghunatha Reddy, A.K.; Goulet, M.-A.; Zaghib, K. Water-in-Salt Electrolytes: Advances and Chemistry for Sustainable Aqueous Monovalent-Metal-Ion Batteries. *Batteries* **2025**, *11*, 120. <https://doi.org/10.3390/batteries11040120>

**Copyright:** © 2025 by the authors. Licensee MDPI, Basel, Switzerland. This article is an open access article distributed under the terms and conditions of the Creative Commons Attribution (CC BY) license (<https://creativecommons.org/licenses/by/4.0/>).

## 1. Introduction

Global energy consumption has surged in recent years, driven by increased demand from various sectors [1]. Human civilization has undergone several energy transitions (Figure 1), with the most recent shift towards renewable energy sources. To meet the increasing global energy demand while minimizing environmental impact, renewable sources such as wind, solar, and tidal power are crucial [2–4]. However, the intermittent nature of these sources necessitates effective energy storage solutions. Energy storage systems can be broadly classified into chemical, mechanical, electrical, and electrochemical categories [5–9]. Among these, electrochemical systems, such as batteries, are particularly well suited for portable applications and electric vehicles [10–12]. These systems store energy through reversible electrochemical reactions involving electrochemically active materials. Batteries present safety concerns due to the risk of thermal runaway [13,14]. Additionally, the cost of batteries is closely tied to the availability of their raw materials. Therefore, ideal battery components should be both inexpensive and non-flammable.

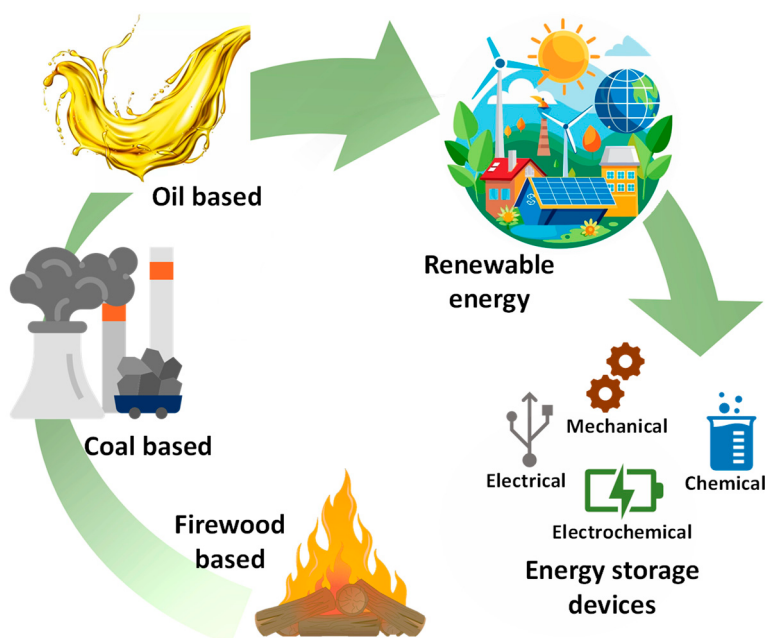


**Figure 1.** Energy transitions and energy storage devices.

Lithium-ion batteries (LIBs), introduced in the 1970s, have become popular for powering everyday gadgets [10,11,15,16]. While LIBs offer impressive performance, they may not be the optimal solution for large-scale energy storage in the context of a third energy transition. LIBs typically employ a graphite anode for lithium-ion intercalation and a metal oxide cathode. Lithium ions move through an organic electrolyte solution containing lithium salts. While widely used, LIBs face limitations in terms of cost and safety. Using expensive metals such as nickel, cobalt, and lithium in the cathode significantly increases the overall cost [17]. Moreover, the growing demand for lithium, projected to reach 54,000 tons annually by 2050 in the United States, is constrained by limited global reserves. In the last decade, this surge in demand has affected lithium carbonate ( $\text{Li}_2\text{CO}_3$ ) prices. Prices were stable from 2010 to 2015 and have since started increasing due to the popularity of EVs and renewable energy storage. The prices increased till 2018, when the supply exceeded demand and then declined. However, a supply deficit in 2022 drastically increased the prices of  $\text{Li}_2\text{CO}_3$  to around 80,000 USD/mt [18]. Both reasons have motivated researchers to investigate alternative monovalent ions and electrode materials. In addition, current lithium-ion battery technology is affected by safety concerns arising from flammable organic electrolytes [13,19]. These electrolytes have a narrow thermal stability range, making the battery susceptible to thermal runaway and potential explosions. Additionally, the complex handling of these electrolytes adds to the overall manufacturing cost [20].

These reasons have motivated researchers to explore non-flammable electrolyte options such as the aqueous electrolytes discussed in this review article [21,22]. Overall, these efforts aim to address the challenges of cost, safety, and sustainability. Multiple aqueous metal-ion batteries (AMIBs), including lithium, have been explored lately. The goal is to develop commercially viable, effective electrochemical energy storage devices with comparable or better performance than LIBs. Ideally, these batteries would have a good cycle life and 100% coulombic efficiency. However, material abundance is crucial to upscale the technology beyond the laboratory scale. The most important aim is ensuring the safe operation of these devices, which involves designing safer batteries based on non-toxic components [23,24].

Understanding key electrochemical factors is essential for developing alternatives to LIBs. Key characteristics include cell voltage, capacity, coulombic efficiency, and cycling

stability. Cell voltage is the electric potential difference between electrodes, while capacity measures the total electricity generated during discharge (e.g., a 3 Ah battery delivers 3 A for 1 h) [9,25]. Coulombic efficiency is the ratio of discharge-to-charge capacity within a cycle, while cycling stability refers to the retention of that capacity over several charge-discharge cycles. LIBs typically have a nominal voltage of 3.6 V, with capacities ranging from 2200 to 2800 mAh for laptops to 40 to 100 kWh for EVs. A coulombic efficiency of 100% indicates that the capacity delivered during discharge is completely regained upon charging, and higher cycling stability is required for the longer life of the battery [25,26]. These four parameters are crucial for assessing the performance of a battery since the cell voltage and capacity of a battery provide a measure of energy density, which is of great interest in determining the application of the designed battery [12]. The other two parameters determine the energy efficiency in a battery, which should essentially be high to make full use of the battery.

### 1.1. Monovalent-Metal-Ion Batteries

LIBs operate on an intercalation-based mechanism involving the reversible movement of lithium ions between the anode and cathode during charging and discharging. Many monovalent metal ions, such as sodium ions and potassium ions, can exhibit similar intercalation behavior [8,27–29]. These ions, particularly sodium, offer advantages such as greater abundance and a lower cost than lithium [8,30–32]. Potassium, despite being low-cost due to its larger size, can pose challenges in terms of ion diffusion and electrode stability [30,33]. The lithium ion's small ionic radius and high charge density make it well suited for intercalation-deintercalation processes, allowing for LIBs with efficient electrode kinetics, high theoretical capacity, and long cycle life. Combined with lithium's low reduction potential, this contributes to the excellent performance and success of LIBs [34]. However, despite having a lower theoretical capacity and larger ionic radius, sodium offers significant advantages. Sodium is one of the most abundant metals on Earth, making it widely available and cost-effective. The challenges associated with lower capacity and slower ion kinetics of sodium can be addressed through advanced electrodes that can potentially accommodate volume changes and provide higher theoretical capacities. While sodium-ion batteries (SIBs) currently exhibit lower energy density than LIBs, they can potentially become a viable and sustainable alternative for various applications, particularly in large-scale energy storage systems. Therefore, sodium-ion batteries have recently gained popularity [35–37]. As of 2020, global potassium reserves were estimated at around 250 billion tons. Unlike lithium, which is concentrated in specific regions such as South America, potassium resources are more evenly distributed worldwide [38,39]. This widespread availability, combined with the lower cost of potassium-based materials, makes potassium-ion batteries (PIBs) an interesting alternative to LIBs. PIBs operate on a similar intercalation mechanism as lithium-ion batteries, involving the reversible transport of ions between the two electrodes. However, potassium ions are larger and have a lower standard redox potential than lithium ions [38]. Despite these differences, potassium's lower Lewis acidity and higher degeneracy energy in certain electrolytes can lead to fast ion diffusion and higher charge-discharge rates [40]. While PIBs offer potential advantages, challenges remain. The large size of potassium ions can cause significant volume expansion in the electrode materials during cycling, which leads to structural instability [41]. Additionally, the higher redox potential of potassium can contribute to electrolyte decomposition [40]. To overcome these limitations, extensive research is required to develop advanced electrode materials that can accommodate the larger ion size and provide stable performance. Despite growing interest in PIBs, lithium-ion batteries dominate the energy storage market and remain the subject of significant research and development efforts [38,42]. A basic

comparison of these systems may include their ionic sizes, reduction potential, Earth abundance, and theoretical capacity to provide insights into volume expansion, cell voltage, material cost, and energy density. We have compared the cost of  $\text{Li}_2\text{CO}_3$ ,  $\text{Na}_2\text{CO}_3$ , and  $\text{KCl}$  to provide a cost comparison of raw materials used in these battery systems.  $\text{Li}_2\text{CO}_3$  will cost 9106.46 USD/mt in 2025, which suggests that one lithium-ion will cost approximately 0.34 USD [18]. However, it was much more expensive in 2022, at 80,000 USD/mt. Sodium and potassium are abundant in Earth's crust and have a cheaper mining process, resulting in much cheaper material costs of 511 USD/mt for  $\text{Na}_2\text{CO}_3$  (0.027 USD/ $\text{Na}^+$ ) and 318.75 USD/mt for  $\text{KCl}$  (0.023 USD/ $\text{K}^+$ ) as of 2025 [43,44]. Table 1 provides a comparison of LIBs with SIBs and PIBs, and Figure 2 demonstrates a graphical representation of the same.

**Table 1.** Comparison of LIBs, SIBs, and PIBs.

	LIBs	SIBs	PIBs
Ionic size (nm)	0.60	0.95	0.133
Reduction potential (V)	−3.04	−2.713	−2.93
Theoretical capacity ( $\text{mAh g}^{-1}$ )	3861	1166	685
Earth's abundance (% of earth's crust)	0.002	2.6	2.1
Cost of ions (USD/ion)	0.34	0.027	0.023

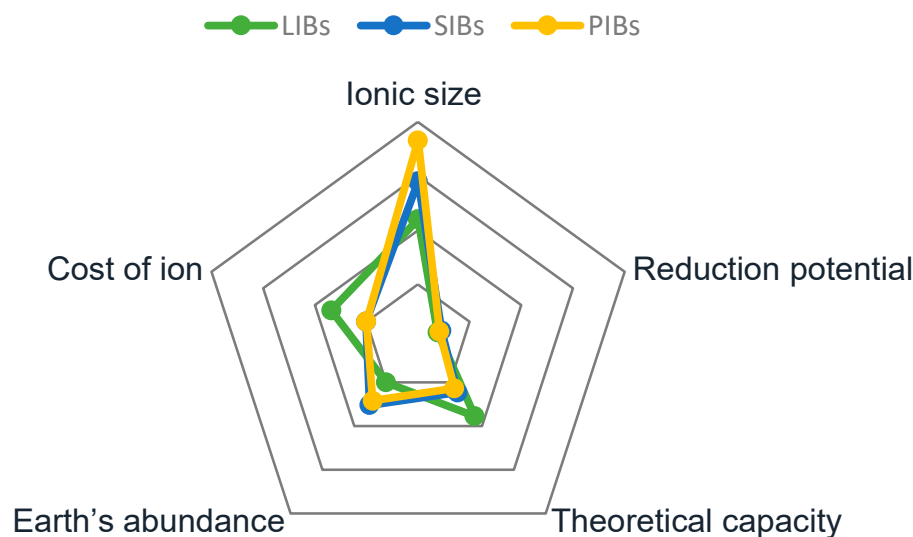


**Figure 2.** Radar plot of comparison between LIBs, SIBs, and PIBs.

## 1.2. Electrolytes

Electrolytes play a vital role in any battery due to their responsibility for ion transport from electrode to electrode. The direct impact of electrolytes on overall battery performance makes them worth investigating. An ideal electrolyte should balance lower viscosity and a higher dielectric constant [45]. A high dielectric constant facilitates salt dissociation, increasing ion solubility, while low viscosity promotes efficient ion transport. The electrolyte must exhibit a wide electrochemical stability window (ESW) to achieve higher cell voltages and prevent side reactions [46,47]. Additionally, the electrolyte should be chemically inert towards all battery components to avoid issues such as electrode dissolution, separator damage, or electrolyte decomposition [48]. An electrolyte should have a low melting point and high boiling point to ensure a broad operational range of temperatures. It should also have a high flash point for safety reasons [12,27,45]. Lastly, to protect the electrode

surface and enable efficient ion transport, the electrolyte should be able to form a stable solid–electrolyte interphase (SEI) layer [49–51].

Metal-ion batteries (MIBs) have primarily relied on organic electrolytes [52–56]. However, a broader range of electrolyte types have been explored, including ionic liquids, aqueous electrolytes, solid polymer electrolytes, and inorganic solid electrolytes [57,58]. The optimal electrolyte for MIBs should ideally possess the characteristics of an ideal electrolyte, such as a high dielectric constant, low viscosity, and a wide electrochemical stability window. While liquid electrolytes generally exhibit higher ionic conductivity than their solid counterparts, research into solid electrolytes is ongoing to address their limitations [38,46,59].

### 1.2.1. Non-Aqueous Electrolytes

Among liquid electrolytes, organic electrolytes commonly used in MIBs are based on cyclic and linear carbonate esters. Cyclic carbonates, such as propylene carbonate and ethylene carbonate, offer high dielectric constants, promoting salt dissociation [60,61]. Linear carbonates, including ethyl methyl carbonate, dimethyl carbonate, and diethyl carbonate, exhibit low viscosities, facilitating ion transport [62,63]. Ethylene carbonate (EC) is a popular organic solvent due to its high dielectric constant, wide thermal stability window, SEI-forming ability, and low volatility. However, its high viscosity limits ionic conductivity. Linear carbonates, while offering lower viscosity, suffer from lower boiling points, lower dielectric constants, and unstable SEI formation. To overcome the limitations of individual carbonate classes, commercial SIBs often employ electrolyte mixtures that combine the advantages of both cyclic and linear carbonates [14,64]. This approach helps balance dielectric constant, viscosity, and electrochemical stability, improving overall performance. These combinations help achieve the benefits of both classes. Organic carbonate mixtures are considered suitable ionic-conducting electrolytes with most of the required qualities achieved via combinations [45,65,66]. Ionic liquids (ILs) are another class of liquid electrolytes composed of bulky, asymmetric cations and anions. This unique structure enables them to exhibit low melting points, high ion densities, wide thermal stability, and broad electrochemical stability windows. However, ILs face challenges such as low ionic conductivity at ambient temperature and potential incompatibility with certain electrode materials. Amongst liquid electrolytes, aqueous electrolytes remain the most conductive electrolyte that can provide cost-effective and safe ion transport in AMIBs [49,67–71].

### 1.2.2. Aqueous Electrolytes

As the name suggests, aqueous electrolytes have water as a solvent. Water is abundant, inexpensive, non-toxic, and fully capable of mitigating safety concerns. Abundant metals such as zinc and iron are being explored in aqueous electrolytes to design sustainable metal-ion batteries. Depending on their redox potentials, many metallic electrodes may corrode in the presence of water [72–74]. This is partly due to the aqueous electrolytes' electrochemical stability window (ESW) limitation of around 1.23 V. This narrow window makes it challenging to pair high-voltage electrode materials (i.e.,  $\text{NaTi}_2(\text{PO}_4)_3 \sim 2.2 \text{ V vs. Na/Na}^+$ ) without triggering side reactions such as hydrogen evolution reaction (HER) or oxygen evolution reaction (OER) [1,38,75]. Apart from the most common barrier of a narrow ESW and corrosion tendency, dendritic growth at some metallic electrodes is commonly observed in aqueous electrolytes. These dendrites may penetrate through separators and eventually cause direct contact between the anode and cathode, which would result in a short circuit of the battery [46,76]. Various strategies have been explored to expand the ESW of aqueous batteries. One approach involves altering the pH of the electrolyte, but this method often leads to control over just one reaction, thereby either suppressing HER or

OER without significantly increasing the overall stability window. Other strategies include constructing artificial interphase layers, increasing electrolyte concentration, and adding electrolyte additives with interphase-forming capabilities [77–79]. Research suggests that stable interphases, along with the expansion of ESW and changes in solvation behavior at high electrolyte concentrations, all help to control corrosion and promote even stripping and plating to avoid dendritic growth [34,80].

### Water-in-Salt Electrolytes

Water-in-salt electrolytes (WiSEs) are a specific type of concentrated electrolyte that has shown promise in widening the ESW of aqueous batteries. As the name suggests, WiSEs have a lower water content than salt in terms of overall composition. By definition, the salt in WiSEs outnumbers the solvent in overall composition by weight and volume [34], which clearly indicates a very low water-to-salt ratio. This unique composition leaves negligible free water molecules in the electrolyte to help mitigate notorious reactions of water with battery components. To achieve these conditions, various solvation sphere alteration approaches have been explored [81,82]. Water can dissolve salt easily due to its high dielectric constant (~78.4 at room temperature), which is greater than the most commonly used organic electrolytes based on propylene carbonates (~64.9 at room temperature). Although this is a useful property for electrolytes, it may also promote the material dissolution of the electrodes [47,83]. However, unlike dilute electrolytes, the minimal amount of water present in WiSEs means that these have a negligible tendency to dissolve electrode material into it.

An important phenomenon present in MIBs with organic electrolytes is the formation of the SEI, which protects the electrodes and enables a wide ESW. Fortunately, similar observations have also been reported for WiSEs by Suo et al. in 2015 [34]. They observed the passivation of the electrodes due to highly concentrated electrolyte composition. This passivation is ionically conductive and electrically insulating. This characteristic of the SEI helps prevent dendritic growth and also protects the electrode from corrosion by water by suppressing the water activity at its surface and thereby mitigating HER and OER [84].

Battery research beyond lithium is crucial for sustainable development in the field of electrochemical energy storage, but every metal-ion battery has its own limitations [38,46,85]. Broadly, aqueous monovalent-metal-ion batteries suffer from unstable SEI, volume change, material dissolution, corrosion, dendrites, OER, and HER [71]. The formation of the SEI in WiSEs and their unique solvation chemistry together helps reduce water activity, expand ESW, and protect the electrodes from corrosion and dendrites along with inhibition of material dissolution, which can potentially enable water as a solvent in metallic and metal-ion battery chemistries (Figure 3) [86]. This review article discusses the development of WiSEs, their SEI formation mechanisms, and their characterizations. The concept of “beyond WiSEs”, which works on a similar mechanism as WiSEs, is also discussed. This review then concludes with a summary and outlook on the prospects for aqueous batteries.

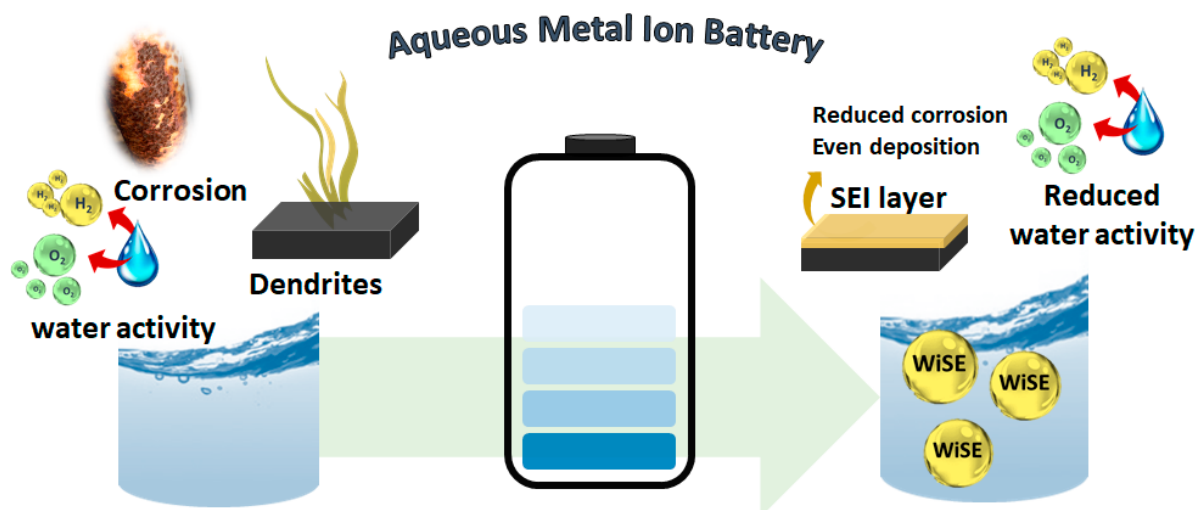


**Figure 3.** Water-in-salt electrolytes mitigate the issues associated with aqueous electrolytes in AMIBs.

## 2. AMIB Components and Compatibility with WiSEs

Suo et al. [34] pioneered the use of water-in-salt electrolytes (WiSEs) in aqueous metal-ion batteries (AMIBs). They demonstrated that a highly concentrated electrolyte could significantly expand the electrochemical stability window of aqueous lithium-ion batteries (LIBs). Prior to that, in 2013, Lux et al. in [1] concluded that lithium bis(trifluoromethanesulfonyl)imide (LiTFSI) offers favorable properties for use in aqueous lithium-ion batteries, including high conductivity, solubility, and thermal stability, but the demonstration of use in batteries was not reported. This super-concentrated electrolyte formed a robust solid-electrolyte interphase (SEI) layer, which improved battery performance and thermal stability. Recognizing the similarities between lithium-ion and sodium-ion batteries, the same research group extended the WiSE concept to aqueous sodium-ion batteries (ASIBs) [80]. Since then, numerous researchers have explored the potential of WiSEs in various metal-ion battery systems, contributing to significant advancements in this field [86–89]. This section outlines the development roadmap for WiSEs in monovalent-metal-ion batteries. It also discusses the battery components, including electrodes, separators, binders, and current collectors, that have been investigated and found to be compatible with WiSEs.

### 2.1. Development of WiSEs

WiSEs have seen significant advancements across various batteries within this short time span. Although their development has followed different paths for different types of batteries, a general pattern can be observed. Initially, efforts were focused on developing WiSE formulations that could form a stable SEI. This was followed by the search for alternative compositions with higher solubility to achieve a higher salt-to-water ratio, which in turn reduced the amount of free water in the electrolyte. Such advancements led to the expansion of ESW. However, the extremely high concentration of electrolytes created a risk of salting out, which redirected research efforts toward developing WiSEs with moderately high concentrations used alongside additives. While the development paths may vary, the overarching goals have remained to enhance the stability and performance of aqueous electrolytes in different battery systems.

#### 2.1.1. Lithium-Ion Batteries (LIBs)

The concept of WiSEs was first introduced in lithium-ion batteries (LIBs) using a 21 m LiTFSI electrolyte [34]. This highly concentrated electrolyte demonstrated SEI formation

and a widened electrochemical stability window (ESW) of 3 V while also exhibiting a conductivity comparable to traditional organic electrolytes. The expanded ESW was attributed to the reduced number of free water molecules due to the high salt concentration. This electrolyte later enabled a 1.75 V symmetric cell using  $\text{TiS}_2$  as an anode and LMO as a cathode [90]. To further increase the concentration, water-in-bisalt electrolytes (WiBSEs) were introduced as a subclass of WiSEs [58]. By combining 21 *m* LiTFSI and 7 *m* LiOTf, a combined molality of 28 *m* was achieved, expanding the ESW to 3.1 V and confirming the concentration dependence of ESW. The electrolyte enabled a 2.5 V cell. Subsequently, the hydrate melt system,  $\text{Li}(\text{TFSI})_{0.7}(\text{BETI})_{0.3}\cdot 2\text{H}_2\text{O}$ , was explored [91], employing lithium salts with bulky anions to reduce the water concentration. These systems exhibit very low water content and have shown promise for high-performance batteries. To develop halide-free electrolytes, non-halide-based salts with high solubility and mixed-cation approaches were investigated. Lukatskaya et al. [20] introduced a mixture of 32 *m* potassium acetate and 8 *m* lithium acetate (32K8Li), achieving a high salt concentration of 40 *m*. However, this electrolyte had a less efficient SEI than imide-based salts, limiting its ESW. Recently, lithium salt monohydrate melts have been explored, pushing the concentration to 55 *m* [92]. Additionally, WiSEs based on lithium (pentafluoroethanesulfonyl) (trifluoromethanesulfonyl) imide have been shown to remain thermodynamically stable in the liquid state down to at least  $-10^\circ\text{C}$  [93]. Becker et al. [93] suggested that this anion is chemically more stable than FSI and FTFSI anions, and lithium bis-(pentafluoroethanesulfonyl) imide (LiPTFSI) exhibits an extremely high solubility of more than 30 *m* at room temperature. Binary mixtures with lithium trifluoromethanesulfonate (LiOTf) can achieve liquidus temperatures as low as  $-14^\circ\text{C}$ .

### 2.1.2. Sodium-Ion Batteries (SIBs)

Recent years have witnessed significant advancements in sodium-ion battery (SIB) technology, driven by the well-established understanding of lithium-ion battery chemistry and the inherent similarities between alkali metal-ion battery mechanisms [65]. Additionally, the cost-effectiveness and intrinsic safety of SIBs make them a promising alternative to lithium-ion batteries [94]. Despite the higher reactivity of sodium, SIBs are considered a safe alternative to LIBs because sodium salts are typically more stable than their lithium counterparts due to their higher Madelung energy, which is related to their electrostatic energy in ionic crystals. For example,  $\text{LiPF}_6$  decomposes at about  $125^\circ\text{C}$ , whereas  $\text{NaPF}_6$  decomposes at around  $325^\circ\text{C}$  [94,95]. For widely used  $\text{NaClO}_4$  in SIBs, the decomposition temperature is  $569.2^\circ\text{C}$ , which is 4.5 times higher than the widely used  $\text{LiPF}_6$  in LIBs. In the case of metallic anodes, sodium dendrites are fluffy due to having lower mechanical strength than lithium dendrites, thereby reducing the chances of short circuits through the separator [94,96]. Suo et al. [80] pioneered the WiSE application in SIBs and LIBs. The first report on WiSEs for SIBs in 2017 by Suo et al. [80] concluded that the Na-ion-conducting SEI layer formation on the  $\text{NaTi}_2(\text{PO}_4)_3$  anode surface was capable of suppressing hydrogen evolution. The electrolyte composition provided an ESW of 2.5 V by combining suppressed OER and HER. The study compared the performance of salt-in-water electrolytes (SiWEs) with that of water-in-salt electrolytes (WiSEs), where the researchers claimed that the coulombic efficiency of the battery with WiSEs reached 100%. When two batteries with identical electrode assemblies were tested in two different electrolyte compositions (SiWEs and WiSEs), the OCV was 1.1 V for each in a charged state. Initially, the OCV dropped from 1.1 to 0.8 in 712 h for WiSEs compared with SiWEs at 540 h when evaluated for self-discharge. Later, the battery was tested for self-discharge in the resting state after multiple cycles in WiSEs. This time, it took more than 940 h to drop its OCV below 1 V due to the robust SEI formed at the anode [80]. The key observation was that  $\text{Na}^+$  could

approach the fluoride ions in electrolytes with a low energy penalty. However, a greater distance between  $\text{Li}^+$  and fluoride ions in the electrolyte demands a higher energy penalty for the Li-F approach [97]. Therefore, sodium salts could form a stable SEI at lower salt concentrations ( $9.26\text{ m}$  NaTFSI) than lithium salts ( $21\text{ m}$  LiTFSI). This SEI formation at lower salt concentrations has increased interest in WiSEs for SIBs. However, a less concentrated electrolyte contains free water molecules, which are prone to water activity and material dissolution. Higher salt concentrations with low water-to-salt ratios reduce the number of free water molecules and consequently expand the ESW. Therefore, researchers have explored salts with higher solubility to further enhance the performance of aqueous sodium-ion batteries (ASIBs). Sodium bis(fluorosulfonyl)imide (NaFSI) is one such salt, offering a solubility of  $21\text{ m}$  at  $23^\circ\text{C}$  [98]. The  $21\text{ m}$  NaFSI electrolyte enabled an ESW of 2.6 V. Inspired by the green and low-cost approach proposed by Lukatskaya et al. [20], researchers investigated a fluorine-free electrolyte mixture consisting of  $32\text{ m}$  potassium acetate (KOAc) and  $8\text{ m}$  sodium acetate (NaOAc) [99]. This super-concentrated electrolyte with a combined concentration of  $40\text{ m}$  significantly reduced the number of free water molecules, effectively suppressing the hydrogen evolution reaction (HER) and oxygen evolution reaction (OER), leading to a wider electrochemical stability window. The wide ESW enabled the pairing of the  $\text{NaTi}_2(\text{PO}_4)_3$  anode with the  $\text{Na}_2\text{MnFe}(\text{CN})_6$  cathode [100]. This combination delivered an average discharge voltage of 0.8 V and a specific capacity of  $37\text{ mAhg}^{-1}$ . This electrolyte composition offers significant advantages in terms of cost reduction and environmental friendliness. To further reduce costs and improve the flammability concerns due to high-concentration organic salts, WiSEs utilizing low-cost inorganic salts such as  $\text{NaClO}_4$  have also been studied by Lee et al. [100]. In this study, the  $17\text{ m}$   $\text{NaClO}_4$  electrolyte expanded the ESW of the electrolyte up to 2.7 V. The cell constructed using a  $\text{Na}_4\text{Fe}_3(\text{PO}_4)_2(\text{P}_2\text{O}_7)$  cathode and a  $\text{NaTi}_2(\text{PO}_4)_3$  anode with this electrolyte composition offered OCV stability of up to 900 h. It also provided 99% coulombic efficiency at 1 C for 200 cycles, which was shown to be comparable to the performance of an equivalent battery utilizing NaTFSI. This performance of the  $\text{NaClO}_4$  electrolyte was delivered due to the formation of an SEI layer composed of  $\text{Na}_2\text{CO}_3$  and  $\text{NaO}$  compounds, including  $\text{Na}_2\text{O}$  and  $\text{NaOH}$ . The discovery of these compounds in the SEI suggested a new mechanism for the SEI formation in ASIBs.

In general, water in bisalt approaches can achieve a higher concentration of salt and thus less free water compared with simple WiSEs. Among WiBSEs, mixed-anion and mixed-cation compositions have been explored. The solubility of mixed cation compositions was typically higher than that of mixed-anion compositions [99,101,102]. In LIBs, mixed-cation approaches are usually less popular due to the risk of co-intercalation. Using inert cations that are too large to co-intercalate can enable a mixed cation approach, which has been demonstrated in ASIBs with tetraethylammonium ( $\text{TEA}^+$ ) [101]. In this study, a mixture of  $22\text{ m}$  tetraethylammonium trifluoromethanesulfonate (TEAOTf) and  $9\text{ m}$  sodium trifluoromethanesulfonate (NaOTf) achieved a  $31\text{ m}$  total cation concentration and expanded the ESW to 3.3 V. This high ESW allows more electrode combinations to achieve a stable, low-cost, efficient battery. This electrolyte composition was also studied for suppression of active material dissolution in ASIBs, and it could effectively reduce the vanadium dissolution from the  $\text{Na}_3\text{V}_2(\text{PO}_4)_3$  electrode (0.09% in 20 days), thereby increasing the cycling stability and coulombic efficiency of the battery [83]. Although highly concentrated WiSEs generally allow for increased operating potential and cycling stability, the thermal stability of these batteries may become compromised at low temperatures due to the “salting out” effect. A balance of a stable SEI layer and good salt solubility was explored thereafter. A combination of  $17\text{ m}$   $\text{NaClO}_4$  with  $2\text{ m}$  NaOTf resulted in a  $\text{NaF-Na}_2\text{O-NaOH}$ -based SEI, which could suppress water activity [102]. Sodium ions could

also be paired with sulfur due to their high theoretical capacity and low cost. However, low sodium confinement (material dissolution) and polysulfide shuttling can eventually cause its capacity to decay. Kumar et al. [82,84] reported the use of WiSEs in controlling polysulfide shuttling in a Na-ion–S battery by tuning the interphase.

### 2.1.3. Potassium-Ion Batteries (PIBs)

Although potassium-ion batteries (PIBs) belong to the same category of intercalation batteries, issues associated with volume change are of greater concern in PIBs than in LIBs and SIBs [33]. The electrodes that support the volume change during intercalation of potassium ions are prone to dissolution in aqueous electrolytes [103]. The electrolytes used in PIBs include organic ether-based, FEC additive-based electrolytes, ionic liquids, polymer electrolytes, highly concentrated ones, and WiSEs. WiSEs were first demonstrated in PIBs in 2019, followed by initiatives such as manipulating the solvation structure and weak cation–anion interaction-based electrolytes. Recent advancements in APIBs have addressed key challenges such as electrolyte stability and electrode dissolution. Hu et al. [38] demonstrated the effectiveness of 22 *m* KCF<sub>3</sub>SO<sub>3</sub> as a high-performance electrolyte, enabling the development of a full PIB cell with a wide voltage window of 3 V. This electrolyte effectively suppressed the dissolution of Mn and Fe ions from the Prussian blue analog (PBA) cathode [41]. Various strategies have been explored to improve electrolyte stability further. Alberto et al. [103] successfully suppressed Mn and Fe dissolution by gelling a 20 *m* KAc electrolyte with carboxymethyl cellulose (CMC). Additionally, Xu et al. [41] introduced Fe<sup>3+</sup> ions into the electrolyte, which were incorporated into the crystal structure of the KMnF cathode, stabilizing the electrode material and mitigating Mn<sup>2+</sup> ion dissolution. A novel approach involves using potassium cyano(trifluoromethanesulfonyl)imide (KCTFSI) as an electrolyte salt. KCTFSI exhibits high solubility and low-temperature stability, surpassing other potassium salts. Spectroscopic studies confirmed the preferential coordination of C≡N groups in KCTFSI, contributing to its enhanced properties. Electrolytes based on KCTFSI offer a wide electrochemical stability window and enable the formation of a stable solid–electrolyte interphase (SEI) on the anode [104]. Full cells utilizing KCTFSI-based electrolytes have demonstrated superior charge–discharge performance, particularly at low temperatures. These advancements in electrolyte design and optimization have significantly contributed to developing high-performance and stable aqueous potassium-ion batteries.

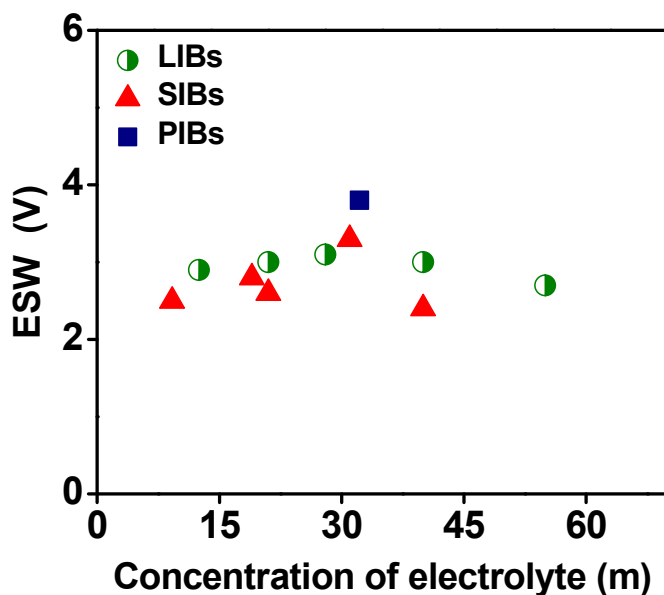
### 2.1.4. Trends in WiSEs

Thus far, WiSEs have expanded the ESW of aqueous electrolytes for AMIBs [98,105–107], controlled material dissolution [82,108], and enabled a variety of electrodes that can be combined to attain a high-voltage battery [50,90,103,109]. Table 2 summarizes the results observed with each chemistry. We have converted the reported anodic and cathodic voltage limits with respect to Ag/AgCl reference for the ease of comparison of ESW across all three battery systems. These ESWs and voltage limits can help in the selection of electrode materials compatible with these electrolytes.

Increasing the electrolyte concentration should increase the salt-to-water ratio and lead to an expanded ESW. As shown in Figure 4, this trend mostly holds true for salt concentrations below 40 *m* for all three battery chemistries but does not for those at or above this value, indicating that there may be diminishing returns to this strategy. Although this area of research is still in its infancy, investigating these parameters more systematically would help develop the stronger trends required to design and optimize successful future AMIBs. There are, of course, many other parameters involved in constructing a successful battery, including electrode materials, separators, and binders, along with current collectors.

**Table 2.** Electrochemical stability window and conductivity of WiSE used in AMIBs.

Battery	Electrolyte Type	Composition	ESW (V)	Anodic-Cathodic Limits (V vs. Ag/AgCl)	Conductivity (mS cm <sup>-1</sup> )	Reference
LIB	WiSE	21 m LiTFSI	3	−1.33 to 1.66	10	[34]
	WiBS	21 m LiTFSI + 7 m LiOTf	3.1	−1.4 to 1.66	6.5	[58]
	Mixed cation	32 m KOAc + 8 m LiOAc	3	−1.3 to 1.7	5.3	[20]
	Monohydrate melt	55 m Li(PTFSI) <sub>0.6</sub> (TFSI) <sub>0.4</sub>	2.7	−0.887 to 1.81	0.1	[92]
	Inert diluent	12.5 m LiNO <sub>3</sub> + PD	2.9	−0.937 to 1.96	0.116	[79]
SIB	WiSE	9.2 m NaOTf	2.5	−1.207 to 1.293	50	[80]
	WiSE	21 m NaTFSI	2.6	−1.15 to 1.45	8	[98]
	WiSE	15 m NaClO <sub>4</sub>	−	−	70	[110]
	Mixed anion	17 m NaClO <sub>4</sub> + 2 m NaOTf	2.8	−1.3 to 1.493	95.25	[102]
	Mixed cation	32 m Kac + 8 m NaAc	−	−	12	[99]
PIB	Inert cation	9 m NaOTf + 22 m TEAOTf	3.3	−1.7 to 1.6	11.2	[101]
	WiSE	32.2 m KCTFSI	3.8	−1.59 to 2.21	28	[104]

**Figure 4.** Trends associated with the solubility of salt and the ESW of WiSEs in AMIBs.

## 2.2. Electrode Materials

The choice of electrodes affects all four of the primary battery metrics discussed previously: cell voltage, capacity, coulombic efficiency, and cycling stability. As cell voltage is directly derived from the electrode potential, coulombic efficiency and cycling stability are related to cell capacity, which is directly proportional to electrode mass [109]. Electrode materials for MIBs must be stable within the electrochemical window, conductive to ions and electrons, cost-effective, high in surface area, and structurally stable to support intercalation and deintercalation. Due to differences in ionic radii, charge density, and ionic mobility, lithium, sodium, and potassium require distinct electrode materials. Common materials such as oxides and PBAs are used across all three systems, but variations in ionic sizes affect volume changes during cycling, leading to different behaviors. For example, APIBs with PBA electrodes outperform ASIBs with PBAs, while ALIBs show poor stability with the same electrode material due to the larger hydrated Li<sup>+</sup> radius [111]. Table 3 provides the performance of electrodes used in AMIBs using WiSE.

### 2.2.1. Lithium-Ion Batteries (LIBs)

Direct utilization of Li as the anode for aqueous batteries is not feasible due to spontaneous HER, necessitating the selection of alternative anode materials. The electrode materials for ALIBs can be categorized into oxides [112,113], polyanionic compounds [114–116], sulfides [108], while some researchers have also explored Prussian blue analogous [111,117–119]. The elementary requirement is smooth intercalation-deintercalation of lithium ions in the matrix. The high conductivity of electrodes is generally beneficial, and cost-effectiveness is crucial. In WiSEs, the full cells assembled for ALIBs include extensive use of  $\text{LiMn}_2\text{O}_4$  as a cathode [34,58,92] with just a few exceptions [20]. Spinels, such as  $\text{LiMn}_2\text{O}_4$ , are the most widely used cathode material, with the advantages of stable skeleton and high safety. Unlike the layered structure,  $\text{LiMn}_2\text{O}_4$  has three-dimensional lithium-ion diffusion channels, and the battery has good low-temperature performance and high safety. Given its olivine structure,  $\text{LiFePO}_4$  is known for its thermal stability, non-toxicity, safety, and low cost. Due to its moderate lithiation/de-lithiation potential (3.5 V vs. Li),  $\text{LiFePO}_4$  has been used in aqueous electrolytes. However, its stability is compromised in alkaline electrolytes or in the presence of dissolved oxygen during charging. Moreover, the narrow electrochemical stability window of aqueous electrolytes limits the choice of anode materials, resulting in aqueous Li-ion full cells using  $\text{LiFePO}_4$  having an output voltage consistently below 1.0 V. The expanded electrochemical stability window offered by WiSEs has enabled the pairing of  $\text{LiFePO}_4$  with  $\text{Mo}_6\text{S}_8$  to create a full cell that benefits from suppressed water activity. The anode materials are usually  $\text{Mo}_6\text{S}_8$ ,  $\text{LiTi}_2(\text{PO}_4)_3$ ,  $\text{TiS}_2$ , and carbon [34,58,90,92,93]. The most popular sulfide anode material is the Chevrel phase  $\text{Mo}_6\text{S}_8$ . Additionally, electrodes with interphase precursor coating have been explored. In such approaches, an immiscible additive and water-based electrolyte can be applied on electrode surfaces, specifically anodes, as a precursor coating for the interphase. The hydrophobic precursor suppresses water reduction during the formation of the interphase. Instead, the precursor undergoes reductive decomposition, creating a hybrid interphase composed of organic and inorganic fluoride compounds. This robust protective layer enables high-capacity and low-potential anode materials to be paired with various cathode materials, thereby expanding the range of choices and possibly enabling high-efficiency ALIBs [120].

### 2.2.2. Sodium-Ion Batteries (SIBs)

A broad classification of electrodes developed in SIBs over the years includes transition metal oxides (TMOs), organic compounds, Prussian blue analogs (PBAs), and polyanion-based materials [31,75,107,121]. TMOs have high energy density and structural versatility, making them popular in intercalation-based batteries. SIBs can take advantage of a variety of cost-effective transition metals that are incompatible with LIBs. Depending on their sodium content, TMOs can be further divided into layered and tunnel-type materials. Highly used layered oxides consist of layers where transition metal oxides and sodium ions are alternatively placed. According to the surrounding environment of sodium in such structures, they are named either P2-type or O3-type. The P2-type layered TMOs are considered ideal cathode materials for SIBs because of their high working voltage and excellent theoretical specific capacity. The P2-type is less packed, thereby providing fast Na-ion diffusion. However, the low sodium content in the P2-type layered TMOs can result in structural deformation, leading to poor cycling performance. The O3-type has greater sodium content and, thus, higher theoretical capacity. However, these layered TMOs require structural tuning through doping to reduce air/moisture sensitivity [85,122]. The tunnel-type layered TMO also supports fast Na-ion diffusion. Their non-toxicity and moderate working voltage with facile synthesis make TMOs compatible with aqueous

electrolytes. Another class of electrodes based on organic compounds can be used with aqueous electrolytes as their potentials lie within the ESW of aqueous electrolytes. These organic electrodes have the potential to become lower-cost and more sustainable options than other electrode materials. For example, Kumaresan et al. [123] reported the synthesis via the solvothermal method of terephthalic acid (TPA) from polyethylene terephthalate (PET) derived from water bottle waste. Using this TPA as a precursor, they synthesized disodium terephthalate ( $\text{Na}_2\text{TP}$ ), and its application as an anode material in SIBs was reported. The most common limitation for organic electrodes is their dissolution in the electrolyte, which may be mitigated with WiSEs. PBAs are another class of electrodes popularly used in SIBs. These are transition metal ferrocyanides with three-dimensional open tunnel structures. This structure enables smooth intercalation–deintercalation, which can accommodate volume changes during cycling. PBAs are known for facile synthesis and abundant sites for ion intercalation, but their moisture sensitivity can lead to water molecules occupying the active sites, which hinders Na ion insertion. This accounts for lowered electrochemical efficiency. Lastly, polyanion-based electrodes are among the most promising electrode materials due to their safety and stability. The infamous sodium supersonic conductors (NASICONs) are part of the polyanion-based electrodes category. These electrodes are stable 3D materials known for facile  $\text{Na}^+$  conductivity. The structures consist of covalent bonds between transition metals and phosphates/silicates/sulfates [49,75]. NASICONs have high ionic conductivity and superior chemical and electrochemical stability. However, it suffers from low electronic conductivity, which can be resolved by combining it with conductive carbonaceous material or doping it with different elements. Furthermore, in the presence of aqueous electrolytes, sodium supersonic conductors suffer from transition metal material dissolution. Some strategies to improve their performance include replacing the vanadium content with other transition metals less prone to dissolution and doping for reducing structural defects [124,125]. Thus far, WiSEs have expanded the electrochemical stability window of electrolytes for ASIBs and thus enabled many categories of electrodes for SIBs in aqueous electrolytes [121].

### 2.2.3. Potassium-Ion Batteries (PIBs)

APIBs have been reported to have electrodes based on PBAs, organic materials, and oxides. However, APIBs using WiSEs have been explored much less, and electrode compatibility has not been specifically reported. The reports so far on APIBs with WiSEs have used  $\text{K}_x\text{Fe}_y\text{Mn}_{1-y}[\text{Fe}(\text{CN})_6]_w \cdot z\text{H}_2\text{O}$  (KFeHCF), 3,4,9,10-perylenetetracarboxylic diimide (PTCDI), and  $\delta\text{-K}_{0.5}\text{V}_2\text{O}_5$  (KVO) [103,104]. While organic electrodes have been used in non-aqueous-based PIBs, their applicability in aqueous electrolytes is constrained by material dissolution. This issue can be tackled via a polymerization approach recently used in APIB using WiSEs. Perylene diimide (PDI) polymers, derived from perylene tetracarboxylic dianhydride (PTCDA), are promising polymerization-based electrode materials for various applications. Their molecular structure allows for customization, enabling control over redox stability, operating potential, and cycling performance, making them attractive for battery applications. As an alternative approach, Suyama et al. transformed  $\alpha\text{-V}_2\text{O}_5$  into KVO “nanobelts” with robust hosting channels and anisotropic pathways for K-ion storage [42]. This structural engineering enhances the material’s performance, improving long-term cyclic stability, high capacity, and higher rate capability. The KVO nanobelt structure offers shorter ion diffusion pathways and increased active sites, resulting in superior K-ion storage capacity compared with untreated  $\text{V}_2\text{O}_5$ . The full cell assembled using KVO and PTCDI in 22 m KOTf was able to deliver high capacity as 95  $\text{mAh g}^{-1}$  at 1 C with 78% capacity retention.

**Table 3.** Performance of electrodes used in WiSE-enabled AMIBs.

Battery	Cathode	Anode	Cell Voltage (V)	Stability (cycles/%retention/c rate)	Energy Density (kWh kg <sup>-1</sup> )	Ref.
LIB	LiMn <sub>2</sub> O <sub>4</sub>	Mo <sub>6</sub> S <sub>8</sub>	2.3	1000/68/4.5	84	[34]
	LiMn <sub>2</sub> O <sub>4</sub>	TiO <sub>2</sub>	2.5	40/91.2	100	[58]
	LiFePO <sub>4</sub>	Mo <sub>6</sub> S <sub>8</sub>	-	1000/99/1	47	[126]
	LiMn <sub>2</sub> O <sub>4</sub>	c-TiO <sub>2</sub>	2.5	55/90		[20]
SIB	LiNi <sub>0.5</sub> Mn <sub>1.5</sub> O <sub>4</sub>	Mo <sub>6</sub> S <sub>8</sub>	2.9	0.075% decay per cycle (5 C)	80	[127]
	LiMn <sub>2</sub> O <sub>4</sub>	Li <sub>4</sub> Ti <sub>5</sub> O <sub>12</sub>	2.5	150/100/0.2	145	[106]
	LiCoO <sub>2</sub>	Mo <sub>6</sub> S <sub>8</sub>	2.5	0.013% decay per cycle (1000)	120	[50]
	Na <sub>2</sub> VTi(PO <sub>4</sub> ) <sub>3</sub>	Na <sub>2</sub> VTi(PO <sub>4</sub> ) <sub>3</sub>	-	No decay (1000 cycles, 20 C)		[124]
PIB	Na <sub>0.66</sub> [Mn <sub>0.66</sub> Ti <sub>0.34</sub> ]O <sub>2</sub>	NaTi <sub>2</sub> (PO <sub>4</sub> ) <sub>3</sub>	1	0.006% decay per cycle (1200 cycles, 1 C)	31	[80]
	Na <sub>1.88</sub> Mn[Fe(CN) <sub>6</sub> ] <sub>0.97</sub> ·1.35H <sub>2</sub> O	NaTiOPO <sub>4</sub>	1.74	200/90/0.25	71	[101]
	Na <sub>4</sub> Fe <sub>3</sub> (PO <sub>4</sub> ) <sub>2</sub> (P <sub>2</sub> O <sub>7</sub> )	NaTi <sub>2</sub> (PO <sub>4</sub> ) <sub>3</sub>	1.08	200/75/1	36	[100]
	K <sub>x</sub> Fe <sub>y</sub> Mn <sub>1-y</sub> [Fe(CN) <sub>6</sub> ] <sub>w</sub> ·zH <sub>2</sub> O	3,4,9,10- perylene tetra carboxylic diimide	1.7	500/88/1	80	[104]
	δ-K <sub>0.5</sub> V <sub>2</sub> O <sub>5</sub>	3,4,9,10- perylene tetra carboxylic diimide		20,000/77.3/10	77.3	[128]

### 2.3. Current Collectors

Current collectors serve as essential components in MIBs, acting as conductive substrates that facilitate electron transport between the active electrode material and the external circuit [129]. These materials must possess exceptional electrochemical stability within the battery's operating voltage range and exhibit robust mechanical properties to withstand the stresses associated with repeated charge–discharge cycles [130–132]. Beyond these fundamental requirements, current collectors significantly influence the overall battery performance, weight, and cost. To meet these demands, current collectors should ideally exhibit high electrical conductivity, excellent electrochemical stability, low density, and abundant availability [129]. A diverse range of materials has been explored for AMIBs, with titanium and stainless steel emerging as prominent choices for WiSE-based AMIBs [34,102]. Apart from these, some WiSE formulations have also enabled the use of aluminum as a current collector in ASIBs [101,110]. Some of these materials have also been combined with others, such as the carbon-coated stainless steel current collectors demonstrated by Wen et al. [133]. While stainless steel was initially employed in early WiSE-based AMIBs, aluminum has gained significant traction due to its high conductivity, low density, and ease of processing [87,131]. The formation of a protective oxide layer on the aluminum surface enhances its oxidative stability, making it a cost-effective and promising candidate [132]. However, aluminum performance is limited by its sensitivity to specific pH ranges and its susceptibility to corrosion in the presence of halides. Recent advancements in halide-free electrolytes, such as those based on potassium and sodium acetate salts, have enabled the utilization of aluminum as a negative electrode in ASIBs. Additionally, the deposition of thin oxide layers, such as Al<sub>2</sub>O<sub>3</sub> and TiO<sub>2</sub>, on current collector surfaces has been shown to expand the ESW, enabling the usage of high-voltage electrode materials such as TiS<sub>2</sub> in ALIBs. Innovative approaches have emerged beyond traditional metallic current collectors, including using conductive polymers, such as conductive vinyl film, and even fully printed

silver current collectors for flexible SIBs [134]. These advancements highlight the ongoing pursuit of advanced current collector materials to optimize the performance, cost, and flexibility of AMIBs.

#### 2.4. Binders

Binders are chemical substances that act as adhesives, securing the electrochemically active material to the surface of the current collector within an electrode [49]. Although constituting a mere 10% of the total electrode mass, these binders play a pivotal role in the electrode's functionality [135,136]. Binders are primarily responsible for binding the active material firmly to the current collector, ensuring a uniform coating and strong adhesion. Additionally, binders must possess electrochemical stability to resist dissolution and facilitate the necessary ion mobility within the electrode [137]. Furthermore, since they are integral to the electrode fabrication, binders must exhibit thermal stability to enable the battery to operate across a wide temperature range. In AMIBs, polymeric binders such as carboxymethylcellulose sodium (CMC), polyvinylidene fluoride (PVDF), polytetrafluoroethylene (PTFE), styrene–butadiene rubber (SBR), and polyvinyl alcohol (PVA) are commonly employed [138,139]. These binders must be compatible with the electrolyte to ensure optimal battery performance. However, in AMIBs utilizing WiSE technology, the role of binders is less extensively researched. Thus far, ALIBs widely use PTFE binders [127,138]. While PVDF and PTFE are the primary binders used in WiSE-based ASIBs, polyacrylic latex is emerging as a potential alternative [102,137,140]. Unfortunately, the binders are inherently electrochemically inactive and possess non-conductive properties that can negatively impact the overall conductivity of the electrode. Moreover, as they comprise nearly 10% of the electrode mass, their inactivity decreases the battery's energy density. To mitigate these limitations, current research is focused on developing self-standing, binder-free electrodes that eliminate the capacity loss associated with the inactive mass of traditional binders [141,142]. The traditional electrode fabrication process involves mechanical grinding of active material with conductive substance and binder followed by coating the slurry on current collectors. This results in weak physical adhesion between the material and current collectors, which can be deformed when electrodes are twisted or bent. During battery cycling, volume expansion can cause the active material to lose electrical contact with the current collector [143]. Binder-free approaches involve the direct deposition of active material on current collectors without the assistance of binders. These can provide a direct charge transport pathway and expose the active sites [141,142].

#### 2.5. Separators

Due to the direct interaction and ion transport responsibility of liquid electrolytes, an ideal separator is a crucial component in battery technology, playing a pivotal role in ensuring optimal performance and safety. It must possess a robust structure capable of withstanding the mechanical, chemical, and thermal stresses inherent to battery operation. Simultaneously, it must exhibit high wettability to efficiently absorb and retain electrolytes, facilitating the rapid and efficient transport of ions between the two electrodes [144–146]. To prevent catastrophic short circuits of the battery, however, an ideal separator would be capable of forming a protective, non-porous layer at highly elevated temperatures, effectively blocking ion transport and safeguarding the battery [147]. Additionally, the separator's pore structure should be uniform, ensuring consistent and efficient ion transport throughout the battery during normal operation. The thickness of the separator is another critical factor, as it influences both ion conductivity and mechanical strength. Thinner separators generally offer superior ion conductivity, leading to higher energy density, but must also possess sufficient mechanical strength to prevent damage during cell assembly and opera-

tion. Ultimately, the ideal separator must strike a balance between these diverse properties, offering robust performance, safety, and cost-effectiveness. WiSE-enabled AMIBs use glass fiber (GF) separators at the lab scale, which have good wettability even at high electrolyte concentrations, thermal stability, and chemical stability. However, they generally have non-uniform pores and lack the mechanical strength required to scale up the technology. However, modified GF separators and novel separator designs have been increasingly explored for AMIBs. These novel separators often possess inherent multifunctional capabilities such as good ion conductivity and mechanical strength due to their functional groups [35,145,146]. Water-in-salt electrolytes (WiSEs) exhibit poor wettability on carbon surfaces of widely used separators such as polyethylene and polypropylene, limiting their application in energy storage devices. Another approach to address this challenge was the development of a novel hydrophilic separator based on cellulose succinate nanofibers (SC-NFs), which involved modifying cellulose through esterification with succinic anhydride, followed by microfluidization to obtain SCNFs. Introducing carboxylate groups onto the cellulose backbone enhances the surface charge density of the nanofibers. This increased negative charge promotes strong electrostatic repulsion between the fibrils, improving electrolyte wettability and facilitating ion transport within the separator [148].

### 3. The Function of WiSEs in AMIBs

The primary benefit of water-in-salt electrolytes (WiSEs) in aqueous metal-ion batteries (AMIBs) is the formation of a solid–electrolyte interphase (SEI) layer, a phenomenon that was first discovered and leveraged in non-aqueous batteries [149]. The SEI is an anodic passivation, which is conductive to ions and electronically insulated. It is formed by the decomposition of electrolyte components at a potential prior to the intercalation potential of metal ions [49,97]. The problem with the formation of the SEI in AMIBs is due to three main factors. First, the decomposition products of water, such as hydrogen, oxygen, hydroxide, and protons, do not readily form a solid deposit on the electrode surface. Secondly, if the SEI forms, it is readily soluble in aqueous electrolyte. For instance, LiF, despite being the least soluble salt of lithium, is soluble in water (approximately 0.04 mol/L) [97]. Lastly, the SEI formation competes with the hydrogen evolution reaction (HER) at the anode due to the narrow electrochemical stability window (ESW) of aqueous electrolytes [97]. The advent of WiSEs has enabled the formation of stable SEI layers in aqueous batteries. WiSEs create a unique electrochemical environment that promotes the formation of a robust SEI layer by significantly increasing the salt concentration in the electrolyte. Typically, the effect of the SEI is observed through enhanced battery performance after the first few cycles since these interphases form during the cycling of the battery [97]. These interphases have a critical role in stabilizing the electrochemically active mass at the electrode throughout the rigorous charge–discharge cycles of a battery at dynamic current rates [83,150]. Numerous factors, including the electrolyte composition, temperature, current density, and electrode material properties, influence the properties of the SEI. In terms of the electrolyte composition, the salts, solvents, and additives can all significantly impact the SEI's morphology, composition, homogeneity, and mechanical properties [49,151]. For instance, fluoride-based salts promote the formation of stable and robust SEI, but non-fluoride-based compositions are observed to form carbonate and oxide or hydroxide-rich SEI layers, which are generally less stable [152].

As the SEI formation competes with HER, having an electrolyte with wider ESW is beneficial. WiSEs offer a unique solvation environment where the free water molecules in electrolytes are significantly decreased. This leads to lowered adsorption of water molecules on the electrode surface, which is a prerequisite for water decomposition reactions. Highly concentrated electrolytes disrupt the hydrogen bonding network of water molecules, re-

ducing water activity and mobility. This change in the solvation environment encourages the formation of ion pairs and aggregates, shifting from solvent-separated ion pairs (SSIPs) to cation–anion aggregates (AGGs) and contact ion pairs (CIPs) [80]. In contact ion pairs, the anions are close to metal ions, which ensures their participation in the formation of the SEI during the intercalation of metal ions. Figure 5 shows the function of WiSEs, i.e., tuning the solvation and promoting the formation of the SEI.

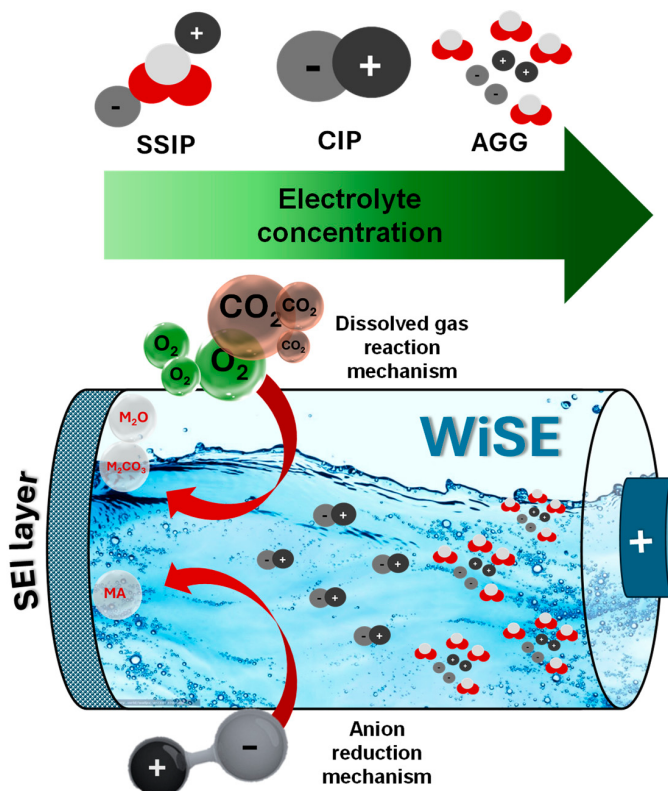


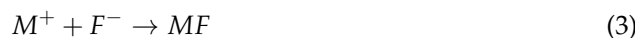
**Figure 5.** Unique solvation offered by WiSE promotes the formation of SEI in AMIBs.

Initial studies on WiSEs for lithium-ion batteries (LIBs) revealed the formation of an SEI when using highly concentrated electrolytes. The LiTFSI- $\text{H}_2\text{O}$  system exhibits wide ESW due to stable LiF-rich SEI formed at anodes. Later, SIBs witnessed similar results with NaOTf- $\text{H}_2\text{O}$ , where this interphase composed of NaF formed at a much lower salt concentration. Molecular dynamics simulations further supported these findings, predicting a high degree of ion pairing and aggregation in the system when compared with LiTFSI- $\text{H}_2\text{O}$ . Further, ALIBs and ASIBs have witnessed oxides and carbonate-based SEI formation without halides using low-cost and safe inorganic salts via a unique mechanism [99,153].

### 3.1. Anion Reduction Mechanism

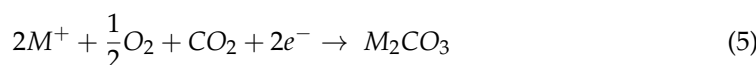
During salt reduction, the anionic part of salt reduces and combines with metal ions at the anode to form an interphase [49,97]. For instance, the OTf moiety of NaOTf reduces to a fluoride ion, which further interacts with sodium ions to form a sodium fluoride-rich interphase, which produces a robust SEI in the ASIB [80]. This mechanism can be generalized for AMIBs with other monovalent metals, as in the following reactions, where the reduction of the salt anion is represented by reactions (1) and (2), and the formation of the SEI is represented by reaction (3).





### 3.2. Dissolved Gas Reaction Mechanism

Other products, such as metal hydroxides and metal carbonates, can also become part of the interphase [110]; dissolved gas reactions form these products. Aqueous electrolytes often include gases such as carbon dioxide and oxygen, which can combine with metal ions at the anode to form such interphases through the following reactions [78,81,97,151,154].



Therefore, these interphases consist of metal oxides (reaction (4)), metal carbonates (reaction (5)), and metal hydroxides (reaction (6)).

In summary, WiSEs change the solvation properties of the electrolyte and drive the formation of AGGs and CIPs. These CIPs and AGGs ensure the participation of anions in interphase formation. Additionally, the presence of free water and its mobility is reduced at such high concentrations, which leads to lesser water adsorption at the electrode, thereby limiting the HER. Lastly, the high concentration of WiSEs helps to avoid the dissolution of the SEI formed. Overall, WiSEs encourage the formation of the SEI by changing solvation, controlling the HER, and limiting its dissolution.

## 4. Characterization Techniques for WiSEs

The definition of water-in-salt electrolytes (WiSEs) specifies that the solute (salt) should be present in greater quantities than the solvent (water), both by weight and volume. This suggests that higher salt concentrations are advantageous, prompting research into salts with increased solubility [20,92,101]. However, salt concentration significantly affects the electrolyte's conductivity and viscosity. Determining the suitability of a WiSE for battery applications requires considering multiple factors, such as salt solubility, conductivity, and the electrolyte's electrochemical stability window (ESW). Computational modeling can predict molecular interactions within the WiSE to understand their solvation properties, which can then be experimentally validated using various spectroscopic techniques. Finally, the solid–electrolyte interphase (SEI) that forms in the assembled battery can be characterized using spectroscopic methods, microscopy, and electrochemical studies to determine its composition, morphology, and resistance. This section details the diverse characterization techniques employed for WiSE analysis. Figure 6 shows the techniques that are used to characterize WiSEs for their preliminary properties, solvation environment, and SEI formation.

### 4.1. Preliminary Testing

Initial electrolyte testing focuses on salt solubility. Highly concentrated electrolytes often exhibit wider ESW due to a reduction in free water molecules [34,80,101]. Mixed-salt approaches are used to enhance solubility [58,101,102], although not all mixtures are effective. For example, a binary mixture of potassium dicyanamide (KDCA) and potassium trifluoromethanesulfonimide (KTFSI) demonstrates lower solubility than either salt individually across all mixing ratios [104]. Salt melting point can be a predictor of solubility as lower melting points suggest lower lattice energy and, thus, higher solubility. Differential scanning calorimetry (DSC) is used to measure melting points. For instance, DSC analysis has shown that in APIBs, KCTFSI has a lower melting point than KTFSI

(133 °C vs. 194 °C), suggesting better solubility. This was confirmed experimentally, with KCTFSI achieving a significantly higher solubility (32.2  $m$ ) compared with KTFSI (1.5  $m$ ) [104]. However, excessively high concentrations can negatively impact conductivity and viscosity. Electrochemical impedance spectroscopy (EIS) is used to measure conductivity. While conductivity typically decreases with increasing concentration, WiSEs can still exhibit conductivity comparable to, or even exceeding, that of non-aqueous electrolytes used in commercial lithium-ion batteries. For example, 21  $m$  LiTFSI has a conductivity of 10 mS cm<sup>-1</sup>, and 9.2  $m$  NaOTf has a conductivity of ~50 mS cm<sup>-1</sup>, while commercial LIB electrolytes have a conductivity of ~9 mS cm<sup>-1</sup> [34,80]. Viscosity, typically measured using viscometers, is often inversely proportional to conductivity at high electrolyte concentrations. However, Ko et al. [92] reported that the monohydrate melt of lithium showed superionic behavior based on a Walden plot, which suggested a faster ionic transport than expected based on viscosity alone.

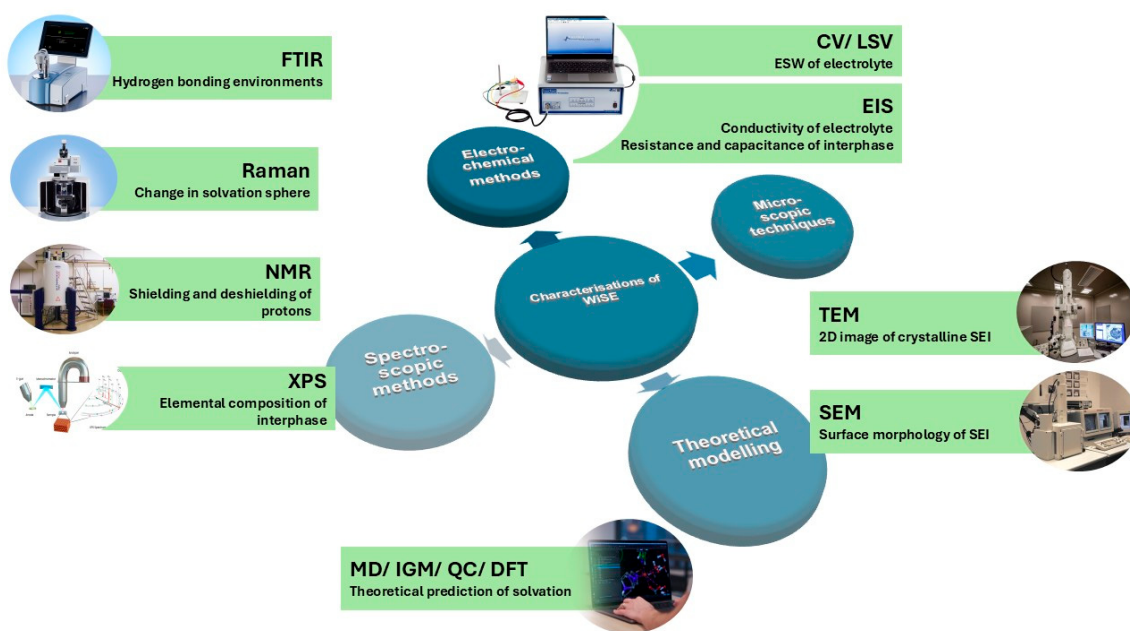


**Figure 6.** Characterization methods for WiSEs for their solvation and the SEI in AMIBs.

The ESW of the electrolyte, on the other hand, is typically determined using linear sweep voltammetry (LSV) or cyclic voltammetry (CV) with bare current collectors. These measurements are performed at slow scan rates (~0.1 mV s<sup>-1</sup>) to simulate real battery conditions [146] better. In the absence of active electrode material, any observed redox peaks indicate water splitting, thus revealing the ESW [34,58].

#### 4.2. Characterization of Solvation

The molecular interaction within electrolytes influences the ESW and SEI formation, as discussed in the previous section. These interactions demonstrate the solvation structure of electrolytes, which drives the formation of the SEI. These solvation spheres can be theoretically modeled, which can be experimentally validated using various spectroscopic methods such as Raman spectroscopy, nuclear magnetic resonance (NMR), and Fourier transform infrared (FTIR) spectroscopy.

##### 4.2.1. Theoretical Calculations

Prior to experiments, theoretical modeling provides valuable predictions about the system. The free energies of solvent-separated ion pairs (SSIPs), contact ion pairs (CIPs), and cation–anion aggregates (AGGs) in electrolytes consisting of water molecules, Na

ions, and OTf ions were calculated using quantum chemistry calculations yielding the lowest free energy for CIPs, which suggested that these interactions might dominate even at lower concentrations in the case of aqueous sodium-ion batteries (ALIBs) [80]. Later, density functional theory (DFT) suggested that the Na ion can approach the F ion with a very low energy penalty compared with the Li-ion approaching the F ion in aqueous lithium-ion batteries (ALIBs) [80]. Molecular dynamics (MD), a computational method used to simulate the physical movements of atoms and molecules, is a valuable tool for understanding the behavior of matter at the atomic and molecular levels. It is known that a solution of hydrated salt can dissolve an unhydrated salt with similar chemical properties and thereby increase the salt concentration and decrease the water-to-salt ratio in the electrolyte. To use this concept in forming a mixed salt electrolyte in ALIBs, 7 *m* LiOTf was added to 21 *m* LiTFSI. MD simulations predicted that approximately 0.5 water molecules are replaced by OTf ions in the Li-ion solvation shell of 21 *m* LiTFSI electrolyte upon the addition of 7 *m* LiOTf, while no significant change is observed on AGGs of Li and TFSI ions [58]. These findings suggested that a mixed-anion approach could be used to lower the water-to-salt ratio in WiSEs by using other ions to replace the water molecules. The Independent Gradient Model (IGM) is another computational chemistry technique designed to visualize and quantify intermolecular interactions. IGM was used to investigate the intermolecular interactions within the NaClO<sub>4</sub>–NaOTf–H<sub>2</sub>O electrolyte. The results indicate that water molecules preferentially interact with ClO<sub>4</sub> and OTf anions through hydrogen bonding, compared with forming water–water clusters. This preferential interaction helps to disrupt the water network and reduce water activity, leading to a more stable electrolyte [102].

#### 4.2.2. Spectroscopic Analysis of Solvation

Various spectroscopic techniques have been used to gain deeper insights into the fundamental properties of electrolytes. Suo et al. [34] reported the Raman spectra for 21 *m* LiTFSI, which revealed a significant broadening of oxygen nuclei peaks at high salt concentrations, suggesting a transition towards a semi-solid state such as crystalline LiTFSI. The cations and anions resembled an ionic liquid environment, where each Li-ion is closely associated with at least one anion. Raman spectroscopy was further employed to investigate the solvation structure of various electrolytes. In NaOTf–H<sub>2</sub>O systems, a significant blue shift in the SO<sub>3</sub> stretching band was observed with increasing salt concentration, indicating a transition from SSIPs to CIPs and AGGs. Figure 7a represents the Raman spectra of electrolytes at different concentrations, suggesting that most of the ions at 9.26 *m* exist as CIPs and AGGs. Figure 7b represents the Raman spectra for NaClO<sub>4</sub>–NaOTf–H<sub>2</sub>O electrolytes, revealing changes in the O–H stretching vibration of water molecules [110]. As the NaClO<sub>4</sub> concentration increased, the band sharpened and blue-shifted, suggesting a disruption of the water structure and the formation of crystalline hydrates. In single-anion electrolytes such as KAc and NaAc, increasing salt concentration decreased water activity, as evidenced by the weakening of the H–O stretching band (Figure 7c) [99]. In APIBs, a KCTFSI-based WiSE was analyzed using Raman spectroscopy, where the significant blue shift in the spectrum from 758.2 to 759.8 cm<sup>−1</sup> (Figure 7d) indicates preferential C≡N coordination across all concentrations. Unlike typical WiSEs, KCTFSI solutions exhibit dominant CIPs even at low concentrations [104].

Fourier transform infrared (FTIR) spectroscopy was employed to examine the interactions between ions and water molecules in various electrolytes. The O–H stretching band, a sensitive indicator of hydrogen bonding networks, was analyzed to understand the changes in solvation structure with increasing salt concentration. The O–H stretching band exhibited a broad peak in pure water due to differences in hydrogen bonding envi-

ronments. As the concentration of salts such as  $\text{NaClO}_4$  increased, the band narrowed and blue-shifted, indicating a disruption of the water structure and the formation of crystalline hydrates (Figure 8a) [80]. In these hydrates, water molecules are strongly coordinated with ions, reducing water activity and mobility. In another report, the addition of additives such as urea and DMF to concentrated electrolytes further modified the solvation structure. The introduction of urea aided the formation of new hydrogen bonds between urea and water molecules, while the addition of DMF further disrupted the hydrogen bonding network [82,84]. FTIR analysis revealed a blue shift in the O–H stretching peaks of water with increasing KCTFSI concentration (Figure 8b), indicating a weakening of hydrogen bonds and increased interaction between water molecules and ions. The C≡N stretching peaks remained relatively unchanged, suggesting preferential coordination of  $\text{K}^+$  ions with C≡N groups even at low concentrations. In contrast, the O=S=O stretching peaks shifted to lower wavenumbers, indicating increased coordination of  $\text{K}^+$  ions with the sulfonyl groups at higher concentrations [104].

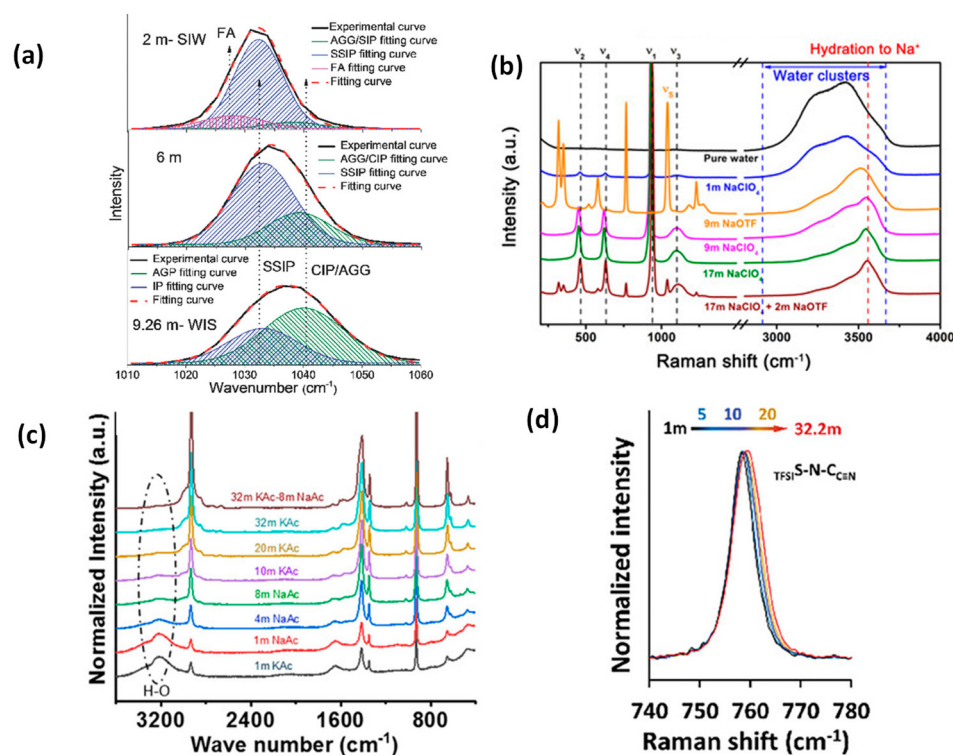


**Figure 7.** Raman spectra for the following: (a) NaWiSEs at different concentrations, reprinted with permission from Ref. [80], copyright 2017 Wiley; (b)  $\text{NaClO}_4$ – $\text{NaOTf}$  mixed-anion WiSE, reprinted with permission from Ref. [102], copyright 2021 Wiley; (c) KAc–NaAc mixed-cation WiSE for ASIB, reprinted with permission from Ref. [110], copyright 2018 Wiley; and (d) KCTFSI WiSE for APIB, reprinted with permission from Ref. [104], copyright 2024 Wiley.

NMR spectroscopy, a technique that exploits the magnetic properties of atomic nuclei, is used to investigate the solvation structure and ion–ion interactions by observing changes in chemical shifts as the electrolyte composition or solute concentration varies.  $^1\text{H}$  NMR spectroscopy was employed to investigate the changes in the water environment with increasing salt concentration. The chemical shift of the water proton shifted upfield with increasing  $\text{NaClO}_4$  concentration, indicating increased shielding by surrounding ions. Similarly, in concentrated  $\text{NaClO}_4$  electrolytes with urea and DMF additives, the upfield shift in the proton signals of water, urea, and DMF suggested decreased water activity and increased interactions between water, salt, and organic additives [84]. In the same electrolyte,  $^{23}\text{Na}$  NMR spectroscopy was employed to investigate the  $\text{Na}^+$  coordination

environment. The upfield shift in the  $^{23}\text{Na}$  NMR signal with increasing salt concentration indicates increased shielding of  $\text{Na}^+$  due to the formation of CIPs, where water molecules are replaced by urea and DMF, leading to a solvation structure with the general formula  $\text{Na}(\text{H}_2\text{O})_x(\text{urea})_y(\text{DMF})_z$  [84]. In another study with 21  $m$  LiTFSI, the  $^{17}\text{O}$  NMR spectra revealed two distinct oxygen environments: water (around 0 ppm) and TFSI<sup>-</sup> (around 154 ppm). The Li-ion interacts with the lone pair of oxygen on water molecules and leads to deshielding, which is pronounced at concentrations higher than 10  $m$ . The signal at 154 ppm is rather unaffected at concentrations below 10  $m$  since TFSI anions do not directly interact with the Li-ion at this point. Above 10  $m$ , both peaks are broadened due to changes in the anion environment, making it similar to crystalline LiTFSI [34].

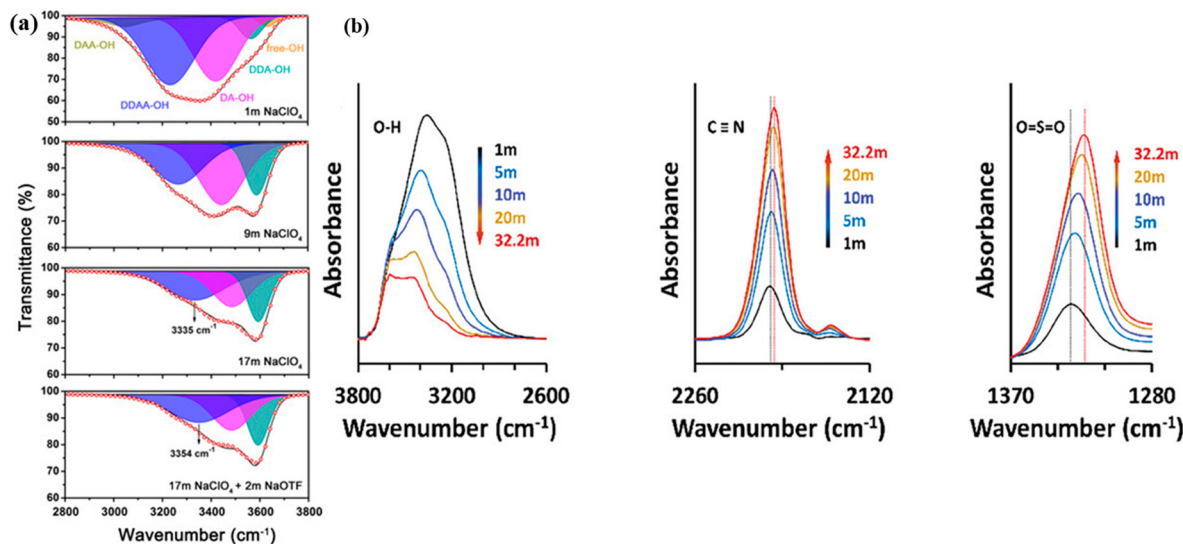


**Figure 8.** FTIR spectra for (a)  $\text{NaClO}_4$ – $\text{NaOTf}$  mixed-anion WiSEs, reprinted with permission from Ref. [102], copyright 2021 Wiley; (b) KCTFSI electrolyte with different concentrations, reprinted with permission from Ref. [104], copyright 2024 Wiley.

#### 4.3. SEI Composition and Properties

The SEI layer is crucial to improve the performance of intercalation batteries. To understand its formation, composition, morphology, and stability, various techniques have been used. Comprehensive SEI characterization requires multiple techniques. X-ray photoelectron spectroscopy (XPS) and energy-dispersive X-ray spectroscopy (EDX) are typically used to determine the elemental composition of the SEI layer, while microscopic methods, including transmission electron microscopy (TEM) and scanning electron microscopy (SEM), are used to gain insights into the surface morphology of the SEI. Finally, electrochemical impedance spectroscopy (EIS) is used to assess the resistance and capacitance of the SEI.

##### 4.3.1. Spectroscopic Analysis of the SEI

XPS can provide information about the elemental composition, chemical state, and electronic structure of the SEI by analyzing the emitted photoelectrons. For instance, Suo et al. [34] employed XPS to investigate the formation of interphase on the anode surface after lithiation by comparing the pristine and lithiated  $\text{Mo}_6\text{S}_8$  electrodes. The spectra revealed significant changes in the elemental composition. In Figure 9a, the disappearance of S 2p and Mo 3d signals and the emergence of Li 1s and F 1s signals after lithiation indicated the formation of a LiF-rich interphase on the anode surface [34]. This interphase was found to be highly resistant to sputtering, suggesting its dense and protective nature. For ASIBs using sodium water-in-salt electrodes (NaWiSEs) and sodium salt-in-water electrodes (NaSiWEs), the NaWiSE electrode exhibited a denser and more robust NaF-rich

SEI compared with the NaSiWE on the anodic surface [80]. In sodium-ion batteries using 19 *m* NaClO<sub>4</sub>–NaOTF electrolytes, XPS analysis indicated the formation of a NaF-based SEI on the anode surface as the position of the Na 1s signal shifts to a higher binding energy (1071.1 eV to 1071.5 eV) after cycling (Figure 9d), indicating the formation of NaF on the surface [102]. In the F1 spectra (Figure 9e), the peak at 689.1 eV for the pristine electrode is of the –CF<sub>2</sub>– group in the polytetrafluoroethylene (PTFE) binder. After cycling, the signal shifts to 678.8 eV, showing the presence of –CF<sub>3</sub>– species from residual salt on the surface. A peak at 684.3 eV emerges after sputtering, corresponding to NaF species. The P 2p spectra (Figure 9f) are provided for reference to show the reappearance of the peak after long-term sputtering, suggesting the robustness of the NaF-based SEI. For NaTi<sub>2</sub>(PO<sub>4</sub>)<sub>3</sub> electrodes cycled in 17 *m* NaClO<sub>4</sub> electrolytes, the electrode exhibited the formation of Na<sub>2</sub>CO<sub>3</sub> and NaOH on the surface, but no NaCl formation was observed, suggesting the mechanism involved is different from salt anion decomposition. These XPS studies provide valuable insights into the composition and properties of SEI layers formed on various electrode materials [102].

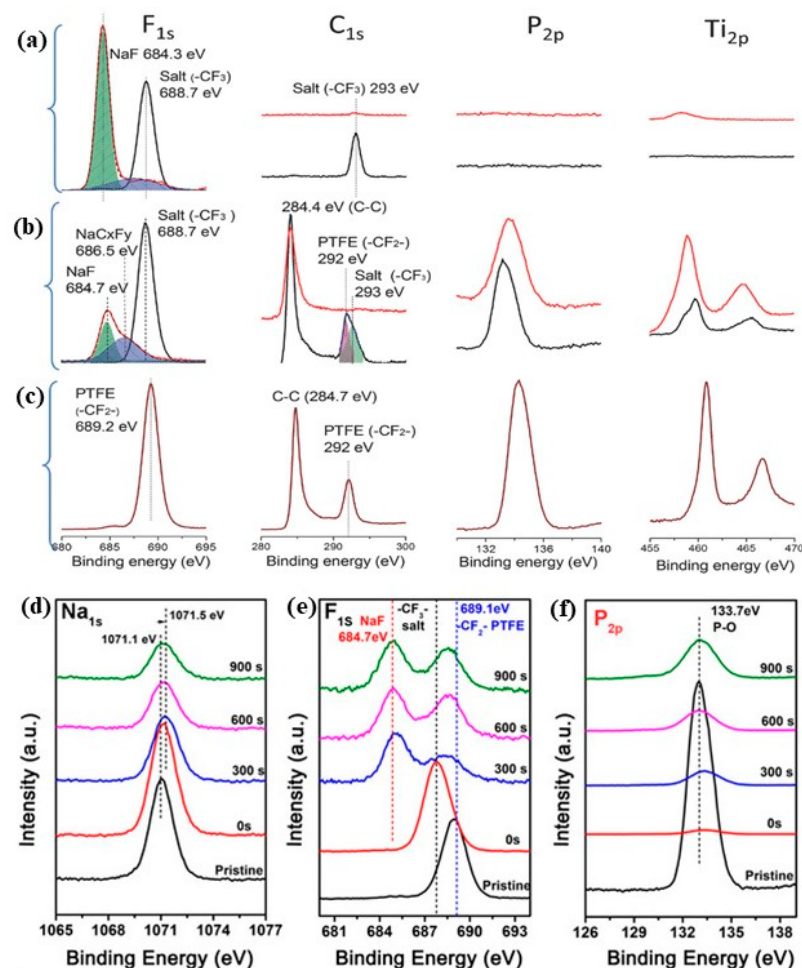


**Figure 9.** XPS spectrum of (a) after 1 cycle in a NaWiSE; (b) after 1 cycle in a NaSiWE. The black and red solid lines represent the cycled electrodes without sputtering and with Ar-ion sputtering for 15 min, respectively. (c) The pristine electrode was reprinted with permission from Ref. [80], copyright 2017 Wiley. (d–f) Pristine and cycled NVP@C anode at full sodiation state after Ar-ion sputtering with different times: (d) Na 1s; (e) F 1s; and (f) P 2p, reprinted with permission from Ref. [102], copyright 2021 Wiley.

#### 4.3.2. Microscopic Studies of SEI Morphology

TEM can produce 2D images at the atomic scale, magnifying nanometre structures up to 50 million times. Thus, the nanoscale SEI can be captured through TEM. To gain insights into the formation of a protective layer on the  $\text{NaTi}_2(\text{PO}_4)_3$  anode, TEM was employed to examine the surface morphology of pristine and cycled electrodes. Pristine  $\text{NaTi}_2(\text{PO}_4)_3$  electrode exhibited clean surfaces (Figure 10a) with a thin carbon coating layer. After cycling the electrode in 17  $m$   $\text{NaClO}_4$  electrolyte, a 5–10 nm thick amorphous layer was observed on the surface, indicating the formation of a protective passivation film [110]. To confirm the formation of the SEI, high-resolution TEM (HRTEM) images of the anode were captured after cycling. Figure 10c,d suggests that, after 1000 cycles at 1 C, an additional layer of partially crystalline material with a thickness of 4–6 nm uniformly covered the surface. The interplanar spacing of this new layer, measured to be 0.25–0.26 nm, closely matches that of crystalline NaF (0.234 nm (200)) [102]. Interestingly, even in a NaSiWE, the SEI layer was observed on the anode particles after 1000 cycles but was less robust than the SEI in NaWiSEs.

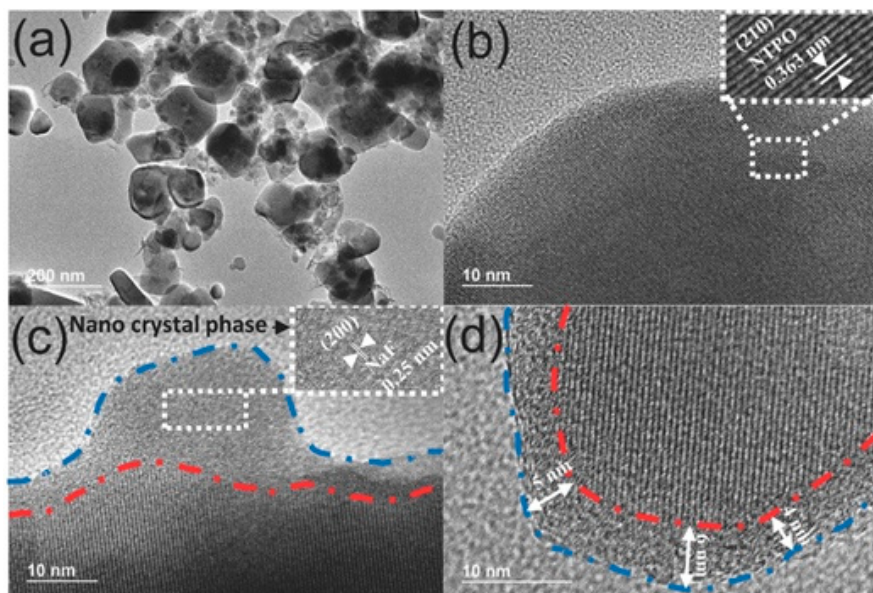


**Figure 10.** TEM images of the  $\text{NaTi}_2(\text{PO}_4)_3$  particle before and after galvanostatic cycling: (a) pristine  $\text{NaTi}_2(\text{PO}_4)_3$  and (b) its high-resolution image; (c) high-resolution images of  $\text{NaTi}_2(\text{PO}_4)_3$  after cycling in a NaWiSE for 421 times at 0.2 C; and (d) after 1000 cycles at 1 C, reprinted with permission from Ref. [80], copyright 2017 Wiley.

In ALIBs, TEM images of the cycled  $\text{Mo}_6\text{S}_8$  revealed a 10–15 nm thick crystalline layer on the surface, which was absent in the pristine material. This layer, identified as imperfect crystalline LiF through interplanar spacing measurements, was further confirmed using EDX analysis, which showed a uniform distribution of fluorine on the  $\text{Mo}_6\text{S}_8$  surface. This aqueous LiF-based SEI, formed by the reduction of TFSI, differs chemically from the composite interphases typically observed in non-aqueous electrolytes, which are primarily composed of solvent-reduction products [34]. Scanning electron microscopy (SEM) is a technique that uses a focused beam of electrons to create high-resolution images of a sample's surface. Agglomerated products can cause the formation of a non-uniform SEI, which leads to uneven ion intercalation through the interphase. The SEM images of the S@MNC-600 electrode cycled in the 17  $m$   $\text{NaClO}_4$  electrolyte revealed a smooth layer on the catalyst surface, identified as  $\text{Na}_2\text{CO}_3$  in ASIBs [84]. This layer formed due to reduced dissolved oxygen and carbon dioxide followed by their reaction with Na ions. An SEI layer was also observed for the  $\text{NaClO}_4$  electrolyte with urea and DMF additives. In the

case without the addition of urea, the SEI was less stable due to cracks resulting from non-uniformity. In the Na–W electrolyte, no SEI was formed at all.

#### 4.3.3. Electrochemical Techniques

EIS measurements have also been conducted to monitor the resistance of the interphase. In a study by Ren et al. [134], EIS revealed that the addition of ethylene glycol (EG) increased the electrolyte resistance but improved the diffusion of Na ions. The authors suggested that the formation of hydrogen bonds between EG and H<sub>2</sub>O reduced the amount of free water, which facilitated Na ion insertion into the electrode material. Solution resistance generally increases using WiSEs. Upon formation of the SEI, the polarization is also expected to increase due to passivation. This increased resistance may resemble delayed corrosion or inhibited parasitic reactions as well.

In summary, the electrolyte is studied for its basic properties, such as its solubility, conductivity, and ESW, using preliminary tests, including EIS and CV/LSV. The cation–anion interactions within the system can be theoretically predicted using MD, IGM, QC, and DFT. Experimentally, the solvation can be analyzed using various spectroscopic methods, including EIS, FTIR, Raman, and NMR. XPS can provide the elemental composition of the SEI formed, and its morphology can be further studied using microscopic techniques such as SEM and TEM.

### 5. Beyond WiSEs

Water-in-salt electrolytes (WiSEs) are primarily useful for expanding the electrochemical stability window (ESW). This expanded ESW is achieved using a high concentration of salts in the electrolyte composition. Despite their usefulness in the aqueous system, the high cost of salts that are used in large quantities to prepare these super-concentrated electrolytes inevitably leads to higher battery costs. Another issue is their saturated concentrations. At such high concentrations, the electrolytes may face salting out at a slight lowering of temperature [42,86]. This limits the use of such electrolytes in a wide temperature range. To achieve a composition that can enable battery operation in a wide temperature range at a low cost, WiSEs with additives to overcome the limitations of salting out have been recently explored. These electrolytes have moderately high, but comparatively lower, salt concentrations, which may also address the issue of high salt costs. The first approach has been the use of salts with anti-freezing properties. Pyrophosphate salts, such as K<sub>4</sub>P<sub>2</sub>O<sub>7</sub>, have been shown to exhibit glass-forming properties and inhibit water freezing [42]. It was found that concentrated K<sub>4</sub>P<sub>2</sub>O<sub>7</sub> electrolytes not only possess the typical characteristics of WiSEs, including an expanded ESW and inhibited aluminum dissolution, but also demonstrate exceptional low-temperature stability, even near the solubility limit. Crowding agents have been used as a second approach to reduce free water molecules. In WiSEs, the formation of cation–anion aggregates (AGGs) and contact ion pairs (CIPs) is attained through a fine balance of electrostatic interactions inside and outside of the solvation shell, where a stronger interaction outside the shell would lead to these ions being pulled towards the exterior of the shell. Nian et al. [81] suggested that increasing salt concentrations would equally increase inward and outward interactions. According to their study, it would be beneficial to establish a protective shell outside the solvation sphere that could potentially hinder the outward interactions. They developed a novel overcrowded electrolyte for aqueous lithium-ion batteries (ALIBs) using the non-polar solvent 1,4-dioxane (DX) as a crowding agent, which interacted with water molecules through hydrogen bonding to form a protective shell around the solvation sphere. Lastly, a third approach has been the use of concentrated diluent wherein inert solvents are used to establish a localized WiSE where the solvents dissolve water but not the salt in the electrolyte. To prepare such

a solution, the solvent should ideally have higher miscibility with water and lower salt solubility to selectively dissolve the water in the solvent. Ethylene carbonate (EC) and 1,5-pentanediol (PD) are such examples. Jaumaux et al. [79] demonstrated the use of PD as a diluent to create a localized WiSE. They also discussed the use of tetraethylene glycol diacrylate (TEGDA) monomer to gel the localized WiSE, which further expanded the ESW of the localized WiSE. Other approaches have involved using polymer additives and constructing an artificial solid–electrolyte interphase (SEI) at the anode along with WiSEs [33,36,78,150,155,156]. However, to the best of our knowledge, no comprehensive comparison of all such systems has been reported thus far.

## 6. Summary and Outlook

The increasing demand for renewable energy has led to a focus on electrochemical energy storage methods, such as metal-ion batteries (MIBs). However, traditional MIBs using organic electrolytes are costly and pose safety risks due to their flammability. Aqueous metal-ion batteries (AMIBs) offer a cost-effective alternative by using water as the solvent, eliminating the requirement for stringent manufacturing conditions and reducing moisture sensitivity. Despite these advantages, AMIBs face challenges such as a narrow electrochemical stability window (ESW) and unstable solid–electrolyte interphases (SEIs).

Water-in-salt electrolytes (WiSEs) are a promising solution to these issues. WiSEs are super-concentrated solutions that reduce water activity, leading to a wider ESW and facilitating SEI formation at the anode. This is achieved through unique solvation structures and reduced free water content due to an increased salt-to-water ratio in the electrolyte, which can increase the ESW. However, the lack of systematic studies varying and reporting this ratio limits our ability to determine strong trends. Correlating electrolyte concentration with ESW thus far suggests that a 3 V wide ESW can be achieved in ASIBs at concentrations below 30  $m$ , whereas it takes more than 30  $m$  concentration to establish the same in ALIBs. To date, there have been a broad range of studies on salts with higher solubility forming WiSEs and expanding the ESW of AMIBs. However, such a high concentration of salts would lead to an increased cost of electrolytes. It is not clear at this early stage whether shifting the cost of the electrolytes from the solvent to the salt will lead to overall cost reductions, and a techno-economic analysis may be warranted. Another issue with using extremely high concentrations of salts is the limited thermal operating window due to the chances of salting out at lower temperatures. To overcome this obstacle, anti-freezing salts, crowding agents, and diluents as additives have been explored. These approaches can enable an SEI at lower salt concentrations, but it remains to be seen whether the stability of this SEI will be compromised due to the risk of dissolution at these lower concentrations. Lastly, it is noteworthy that the recent developments in WiSEs have expanded the ESW of aqueous electrolytes up to 3.6–4 V, yet no AMIBs have been demonstrated to fully utilize such an expanded ESW due to a lack of compatible electrode materials. Therefore, further research is required to address the compatibility of electrodes with WiSEs to take advantage of this technology. Overall, much progress has been made in AMIBs using WiSEs, with the most significant advancement being the establishment of a stable SEI. This significant result is a promising start for this new approach that may eventually enable safer and lower-cost batteries to accelerate the energy transition.

**Author Contributions:** R.N.M. drafted the manuscript and produced the graphics. M.-A.G. edited the manuscript. A.K.M.R.R., M.-A.G. and K.Z. designed the overall structure of the review, with all authors contributing equally. All authors have read and agreed to the published version of the manuscript.

**Funding:** This research was supported by a Discovery Grant from the Natural Science and Engineering Research Council of Canada (RGPIN-2022-04670) and Ministry of Economy, Innovation and Energy Québec.

**Acknowledgments:** The authors thank NSERC CRSNG and the Ministry of Economy, Innovation and Energy Quebec for their financial support.

**Conflicts of Interest:** The authors declare no conflicts of interest.

## References

1. Lux, S.F.; Terborg, L.; Hachmöller, O.; Placke, T.; Meyer, H.-W.; Passerini, S.; Winter, M.; Nowak, S. LiTFSI Stability in Water and Its Possible Use in Aqueous Lithium-Ion Batteries: pH Dependency, Electrochemical Window and Temperature Stability. *J. Electrochem. Soc.* **2013**, *160*, A1694–A1700. [[CrossRef](#)]
2. Bogdanov, D.; Ram, M.; Aghahosseini, A.; Gulagi, A.; Oyewo, A.S.; Child, M.; Caldera, U.; Sadovskaya, K.; Farfan, J.; De Souza Noel Simas Barbosa, L.; et al. Low-Cost Renewable Electricity as the Key Driver of the Global Energy Transition towards Sustainability. *Energy* **2021**, *227*, 120467. [[CrossRef](#)]
3. Child, M.; Koskinen, O.; Linnanen, L.; Breyer, C. Sustainability Guardrails for Energy Scenarios of the Global Energy Transition. *Renew. Sustain. Energy Rev.* **2018**, *91*, 321–334. [[CrossRef](#)]
4. Solomon, B.D.; Krishna, K. The Coming Sustainable Energy Transition: History, Strategies, and Outlook. *Asian Energy Secur.* **2011**, *39*, 7422–7431. [[CrossRef](#)]
5. Bhojane, P. Recent Advances and Fundamentals of Pseudocapacitors: Materials, Mechanism, and Its Understanding. *J. Energy Storage* **2022**, *45*, 103654. [[CrossRef](#)]
6. Chodankar, N.R.; Pham, H.D.; Nanjundan, A.K.; Fernando, J.F.S.; Jayaramulu, K.; Golberg, D.; Han, Y.-K.; Dubal, D.P. True Meaning of Pseudocapacitors and Their Performance Metrics: Asymmetric versus Hybrid Supercapacitors. *Small* **2020**, *16*, 2002806. [[CrossRef](#)]
7. Wu, H.; Xie, G.; Jie, Z.; Hui, X.; Yang, D.; Du, C. Research Progress about Chemical Energy Storage of Solar Energy. *IOP Conf. Ser. Earth Environ. Sci.* **2018**, *108*, 052070. [[CrossRef](#)]
8. Pan, Q.; Tong, Z.; Su, Y.; Qin, S.; Tang, Y. Energy Storage Mechanism, Challenge and Design Strategies of Metal Sulfides for Rechargeable Sodium/Potassium-Ion Batteries. *Adv. Funct. Mater.* **2021**, *31*, 2103912. [[CrossRef](#)]
9. Zhu, W.H.; Zhu, Y.; Davis, Z.; Tatarchuk, B.J. Energy Efficiency and Capacity Retention of Ni–MH Batteries for Storage Applications. *Appl. Energy* **2013**, *106*, 307–313. [[CrossRef](#)]
10. Wang, Y.; Liu, B.; Li, Q.; Cartmell, S.; Ferrara, S.; Deng, Z.D.; Xiao, J. Lithium and Lithium Ion Batteries for Applications in Microelectronic Devices: A Review. *J. Power Sources* **2015**, *286*, 330–345. [[CrossRef](#)]
11. Choi, S.; Wang, G. Advanced Lithium-Ion Batteries for Practical Applications: Technology, Development, and Future Perspectives. *Adv. Mater. Technol.* **2018**, *3*, 1700376. [[CrossRef](#)]
12. Deng, J.; Bae, C.; Denlinger, A.; Miller, T. Electric Vehicles Batteries: Requirements and Challenges. *Joule* **2020**, *4*, 511–515. [[CrossRef](#)]
13. Arbizzani, C.; Gabrielli, G.; Mastragostino, M. Thermal Stability and Flammability of Electrolytes for Lithium-Ion Batteries. *J. Power Sources* **2011**, *196*, 4801–4805. [[CrossRef](#)]
14. Kawamura, T.; Kimura, A.; Egashira, M.; Okada, S.; Yamaki, J.-I. Thermal Stability of Alkyl Carbonate Mixed-Solvent Electrolytes for Lithium Ion Cells. *J. Power Sources* **2002**, *104*, 260–264. [[CrossRef](#)]
15. Blomgren, G.E. The Development and Future of Lithium Ion Batteries. *J. Electrochem. Soc.* **2017**, *164*, A5019–A5025. [[CrossRef](#)]
16. Kim, T.; Song, W.; Son, D.-Y.; Ono, L.K.; Qi, Y. Lithium-Ion Batteries: Outlook on Present, Future, and Hybridized Technologies. *J. Mater. Chem. A* **2019**, *7*, 2942–2964. [[CrossRef](#)]
17. Zhou, L.; Li, H.; Wu, X.; Zhang, Y.; Danilov, D.L.; Eichel, R.-A.; Notten, P.H.L. Double-Shelled  $\text{Co}_3\text{O}_4/\text{C}$  Nanocages Enabling Polysulfides Adsorption for High-Performance Lithium–Sulfur Batteries. *ACS Appl. Energy Mater.* **2019**, *2*, 8153–8162. [[CrossRef](#)]
18. Lithium Price Today | Lithium Spot Price Chart | Historical Price of Lithium—Shanghai Metal Market. Available online: <https://www.metal.com/en/markets/40> (accessed on 10 March 2025).
19. Swiderska-Mocek, A.; Jakobczyk, P.; Rudnicka, E.; Lewandowski, A. Flammability Parameters of Lithium-Ion Battery Electrolytes. *J. Mol. Liq.* **2020**, *318*, 113986. [[CrossRef](#)]
20. Lukatskaya, M.R.; Feldblyum, J.I.; Mackanic, D.G.; Lissel, F.; Michels, D.L.; Cui, Y.; Bao, Z. Concentrated Mixed Cation Acetate “Water-in-Salt” Solutions as Green and Low-Cost High Voltage Electrolytes for Aqueous Batteries. *Energy Environ. Sci.* **2018**, *11*, 2876–2883. [[CrossRef](#)]
21. Luntz, A. Beyond Lithium Ion Batteries. *J. Phys. Chem. Lett.* **2015**, *6*, 300–301. [[CrossRef](#)]
22. Gao, Y.; Pan, Z.; Sun, J.; Liu, Z.; Wang, J. High-Energy Batteries: Beyond Lithium-Ion and Their Long Road to Commercialisation. *Nano-Micro Lett.* **2022**, *14*, 94. [[CrossRef](#)]

23. de Meatza, I.; Urdampilleta, I.; Boyano, I.; Castrillo, I.; Landa-Medrano, I.; Sananes-Israel, S.; Eguia-Barrio, A.; Palomares, V. From Lab to Manufacturing Line: Guidelines for the Development and Upscaling of Aqueous Processed NMC622 Electrodes. *J. Electrochem. Soc.* **2023**, *170*, 010527. [CrossRef]
24. Molaiyan, P.; Bhattacharyya, S.; Dos Reis, G.S.; Sliz, R.; Paolella, A.; Lassi, U. Towards Greener Batteries: Sustainable Components and Materials for next-Generation Batteries. *Green Chem.* **2024**, *26*, 7508–7531. [CrossRef]
25. Yang, F.; Wang, D.; Zhao, Y.; Tsui, K.-L.; Bae, S.J. A Study of the Relationship between Coulombic Efficiency and Capacity Degradation of Commercial Lithium-Ion Batteries. *Energy* **2018**, *145*, 486–495. [CrossRef]
26. He, H.; Sun, D.; Tang, Y.; Wang, H.; Shao, M. Understanding and Improving the Initial Coulombic Efficiency of High-Capacity Anode Materials for Practical Sodium Ion Batteries. *Energy Storage Mater.* **2019**, *23*, 233–251. [CrossRef]
27. Xu, T.; Yu, J.; Ma, J.; Ren, W.; Hu, M.; Li, X. The Critical Role of Water Molecules in the Development of Aqueous Electrolytes for Rechargeable Metal-Ion Batteries. *J. Mater. Chem. A* **2024**, *12*, 13551–13575. [CrossRef]
28. Gao, H.; Tang, K.; Xiao, J.; Guo, X.; Chen, W.; Liu, H.; Wang, G. Recent Advances in “Water in Salt” Electrolytes for Aqueous Rechargeable Monovalent-Ion ( $\text{Li}^+$ ,  $\text{Na}^+$ ,  $\text{K}^+$ ) Batteries. *J. Energy Chem.* **2022**, *69*, 84–99. [CrossRef]
29. Zuo, W.; Innocenti, A.; Zarzabeitia, M.; Bresser, D.; Yang, Y.; Passerini, S. Layered Oxide Cathodes for Sodium-Ion Batteries: Storage Mechanism, Electrochemistry, and Techno-Economics. *Acc. Chem. Res.* **2023**, *56*, 284–296. [CrossRef]
30. Yuan, M.; Liu, H.; Ran, F. Fast-Charging Cathode Materials for Lithium & Sodium Ion Batteries. *Mater. Today* **2023**, *63*, 360–379. [CrossRef]
31. Slater, M.D.; Kim, D.; Lee, E.; Johnson, C.S. Sodium-Ion Batteries. *Adv. Funct. Mater.* **2013**, *23*, 947–958. [CrossRef]
32. Nayak, P.K.; Yang, L.; Brehm, W.; Adelhelm, P. From Lithium-Ion to Sodium-Ion Batteries: Advantages, Challenges, and Surprises. *Angew. Chem. Int. Ed.* **2018**, *57*, 102–120. [CrossRef]
33. Vardhini, G.; Dilip, P.S.; Kumar, S.A.; Suriyakumar, S.; Hariharan, M.; Shajumon, M.M. Polyimide-Based Aqueous Potassium Energy Storage Systems Using Concentrated WiSE Electrolyte. *ACS Appl. Mater. Interfaces* **2024**, *16*, 48782–48791. [CrossRef]
34. Suo, L.; Borodin, O.; Gao, T.; Olguin, M.; Ho, J.; Fan, X.; Luo, C.; Wang, C.; Xu, K. “Water-in-Salt” Electrolyte Enables High-Voltage Aqueous Lithium-Ion Chemistries. *Science* **2015**, *350*, 938–943. [CrossRef] [PubMed]
35. Zhang, L.; Li, X.; Yang, M.; Chen, W. High-Safety Separators for Lithium-Ion Batteries and Sodium-Ion Batteries: Advances and Perspective. *Energy Storage Mater.* **2021**, *41*, 522–545. [CrossRef]
36. Yang, M.; Luo, J.; Guo, X.; Chen, J.; Cao, Y.; Chen, W. Aqueous Rechargeable Sodium-Ion Batteries: From Liquid to Hydrogel. *Batteries* **2022**, *8*, 180. [CrossRef]
37. Huang, W.; Yang, F.; Xu, G.; Chen, J.; Shi, W.; Yang, Y. Ba-Doped  $\text{Na}_0.16\text{MnO}_2$  with Ultra-Long Cycling Life and Highly Reversible Insertion/Extraction Mechanism for Aqueous Rechargeable Sodium Ion Batteries. *J. Energy Storage* **2024**, *98*, 112983. [CrossRef]
38. He, X.; Iqbal, N.; Ghani, U.; Li, T. Potassium Ion Batteries: Recent Advancements in Anodic, Cathodic, and Electrolytic Materials. *J. Alloys Compd.* **2024**, *981*, 173680. [CrossRef]
39. Hwang, J.-Y.; Myung, S.-T.; Sun, Y.-K. Recent Progress in Rechargeable Potassium Batteries. *Adv. Funct. Mater.* **2018**, *28*, 1802938. [CrossRef]
40. Leonard, D.P.; Wei, Z.; Chen, G.; Du, F.; Ji, X. Water-in-Salt Electrolyte for Potassium-Ion Batteries. *ACS Energy Lett.* **2018**, *3*, 373–374. [CrossRef]
41. Xu, Y.; Ding, T.; Sun, D.; Ji, X.; Zhou, X. Recent Advances in Electrolytes for Potassium-Ion Batteries. *Adv. Funct. Mater.* **2023**, *33*, 2211290. [CrossRef]
42. Suyama, H.; Sato, S.; Matsunaga, T.; Inoue, T.; Ikezawa, A.; Arai, H. Anticrystallization and Superionic Conduction of Highly Concentrated Potassium Pyrophosphate Aqueous Electrolytes. *ACS Appl. Energy Mater.* **2023**, *6*, 11897–11905. [CrossRef]
43. Daily Sodium-Ion Battery Price, Lme Comex Shfe Price of Sodium-Ion Battery Live | SMM—Metal Market. Available online: <https://www.metal.com/Sodium-ion%20Battery> (accessed on 10 March 2025).
44. Potassium Chloride (Muriate of Potash) Spot Price Monthly Insights: Commodity Markets Review | YCharts. Available online: [https://ycharts.com/indicators/potassium\\_chloride\\_muriate\\_of\\_potash\\_spot\\_price](https://ycharts.com/indicators/potassium_chloride_muriate_of_potash_spot_price) (accessed on 11 March 2025).
45. Kalhoff, J.; Eshetu, G.G.; Bresser, D.; Passerini, S. Safer Electrolytes for Lithium-Ion Batteries: State of the Art and Perspectives. *ChemSusChem* **2015**, *8*, 2154–2175. [CrossRef]
46. Burton, T.F.; Jommongkol, R.; Zhu, Y.; Deebansok, S.; Chitbankluai, K.; Deng, J.; Fontaine, O. Water-in-Salt Electrolytes towards Sustainable and Cost-Effective Alternatives: Example for Zinc-Ion Batteries. *Curr. Opin. Electrochem.* **2022**, *35*, 101070. [CrossRef]
47. Chen, H.; Zhang, Z.; Wei, Z.; Chen, G.; Yang, X.; Wang, C.; Du, F. Use of a Water-in-Salt Electrolyte to Avoid Organic Material Dissolution and Enhance the Kinetics of Aqueous Potassium Ion Batteries. *Sustain. Energy Fuels* **2020**, *4*, 128–131. [CrossRef]
48. Liu, Y.-K.; Zhao, C.-Z.; Du, J.; Zhang, X.-Q.; Chen, A.-B.; Zhang, Q. Research Progresses of Liquid Electrolytes in Lithium-Ion Batteries. *Small* **2023**, *19*, 2205315. [CrossRef]
49. Bommier, C.; Ji, X. Electrolytes, SEI Formation, and Binders: A Review of Nonelectrode Factors for Sodium-Ion Battery Anodes. *Small* **2018**, *14*, 1703576. [CrossRef]

50. Wang, F.; Lin, Y.; Suo, L.; Fan, X.; Gao, T.; Yang, C.; Han, F.; Qi, Y.; Xu, K.; Wang, C. Stabilizing High Voltage LiCoO<sub>2</sub> Cathode in Aqueous Electrolyte with Interphase-Forming Additive. *Energy Environ. Sci.* **2016**, *9*, 3666–3673. [CrossRef]
51. Jommongkol, R.; Deebansok, S.; Deng, J.; Zhu, Y.; Bouchal, R.; Fontaine, O. Unveiling LiTFSI Precipitation as a Key Factor in Solid Electrolyte Interphase Formation in Li-Based Water-in-Salt Electrolytes. *Small* **2024**, *20*, 2303945. [CrossRef]
52. Lin, Y.; Peng, Q.; Chen, L.; Zuo, Q.; Long, Q.; Lu, F.; Huang, S.; Chen, Y.; Meng, Y. Organic Liquid Electrolytes in Sodium-Based Batteries: Actualities and Perspectives. *Energy Storage Mater.* **2024**, *67*, 103211. [CrossRef]
53. Mao, J.; Wang, C.; Lyu, Y.; Zhang, R.; Wang, Y.; Liu, S.; Wang, Z.; Zhang, S.; Guo, Z. Organic Electrolyte Design for Practical Potassium-Ion Batteries. *J. Mater. Chem. A* **2022**, *10*, 19090–19106. [CrossRef]
54. Zhang, X.; Cui, Z.; Wei, T.; Wang, W.; Wu, Q.; Fu, Y.; Yang, T.; Wang, J.-R.; Li, H.; Wang, B.; et al. Phosphonitrile Based Porous Organic Polymers as Effective Flame-Retardant Electrolytes for Lithium Battery. *Polymer* **2024**, *311*, 127504. [CrossRef]
55. Ma, G.; Di, S.; Wang, Y.; Yuan, W.; Ji, X.; Qiu, K.; Liu, M.; Nie, X.; Zhang, N. Zn Metal Anodes Stabilized by an Intrinsically Safe, Dilute, and Hydrous Organic Electrolyte. *Energy Storage Mater.* **2023**, *54*, 276–283. [CrossRef]
56. Shyma Sajeevan, A.; Bernard, L.; Tran-Van, P.; Brandell, D.; Renault, S.; Poizot, P. Combining Polyester-Based Solid Polymer Electrolytes with Lithiated Organic Cathodes for 3.5 V-Class Li-Organic Rechargeable Batteries. *ACS Appl. Polym. Mater.* **2024**, *6*, 10102–10112. [CrossRef]
57. Zhu, K.; Li, Z.; Sun, Z.; Liu, P.; Jin, T.; Chen, X.; Li, H.; Lu, W.; Jiao, L. Inorganic Electrolyte for Low-Temperature Aqueous Sodium Ion Batteries. *Small* **2022**, *18*, 2107662. [CrossRef]
58. Suo, L.; Borodin, O.; Sun, W.; Fan, X.; Yang, C.; Wang, F.; Gao, T.; Ma, Z.; Schroeder, M.; von Cresce, A.; et al. Advanced High-Voltage Aqueous Lithium-Ion Battery Enabled by “Water-in-Bisalt” Electrolyte. *Angew. Chem. Int. Ed.* **2016**, *55*, 7136–7141. [CrossRef]
59. Ji, D.; Kim, J. Trend of Developing Aqueous Liquid and Gel Electrolytes for Sustainable, Safe, and High-Performance Li-Ion Batteries. *Nano-Micro Lett.* **2024**, *16*, 2. [CrossRef]
60. Tasaki, K.; Goldberg, A.; Winter, M. On the Difference in Cycling Behaviors of Lithium-Ion Battery Cell between the Ethylene Carbonate- and Propylene Carbonate-Based Electrolytes. *Electrochim. Acta* **2011**, *56*, 10424–10435. [CrossRef]
61. Xing, L.; Li, W.; Wang, C.; Gu, F.; Xu, M.; Tan, C.; Yi, J. Theoretical Investigations on Oxidative Stability of Solvents and Oxidative Decomposition Mechanism of Ethylene Carbonate for Lithium Ion Battery Use. *J. Phys. Chem. B* **2009**, *113*, 16596–16602. [CrossRef]
62. Huang, Y.; Luo, Y.; Wang, B.; Wang, H.; Zhang, L. Crucial Roles of Ethyl Methyl Carbonate in Lithium-Ion and Dual-Ion Batteries: A Review. *Langmuir* **2024**, *40*, 11353–11370. [CrossRef]
63. Yoshida, H.; Fukunaga, T.; Hazama, T.; Terasaki, M.; Mizutani, M.; Yamachi, M. Degradation Mechanism of Alkyl Carbonate Solvents Used in Lithium-Ion Cells during Initial Charging. *J. Power Sources* **1997**, *68*, 311–315. [CrossRef]
64. Seo, D.M.; Reininger, S.; Kutcher, M.; Redmond, K.; Euler, W.B.; Lucht, B.L. Role of Mixed Solvation and Ion Pairing in the Solution Structure of Lithium Ion Battery Electrolytes. *J. Phys. Chem. C* **2015**, *119*, 14038–14046. [CrossRef]
65. Vignarooban, K.; Kushagra, R.; Elango, A.; Badami, P.; Mellander, B.-E.; Xu, X.; Tucker, T.G.; Nam, C.; Kannan, A.M. Current Trends and Future Challenges of Electrolytes for Sodium-Ion Batteries. *Int. J. Hydrogen Energy* **2016**, *41*, 2829–2846. [CrossRef]
66. Karaseva, E.V.; Kuzmina, E.V.; Li, B.-Q.; Zhang, Q.; Kolosnitsyn, V.S. Effect of the Anionic Composition of Sulfolane Based Electrolytes on the Performances of Lithium-Sulfur Batteries. *J. Energy Chem.* **2024**, *95*, 231–240. [CrossRef]
67. Zhang, J.; Yao, X.; Misra, R.K.; Cai, Q.; Zhao, Y. Progress in Electrolytes for Beyond-Lithium-Ion Batteries. *J. Mater. Sci. Technol.* **2020**, *44*, 237–257. [CrossRef]
68. Gallastegui, A.; Lingua, G.; Lopez-Larrea, N.; Carfora, R.; Pasini, D.; Mantione, D.; Mecerreyes, D. Piperazinium Poly(Ionic Liquid)s as Solid Electrolytes for Lithium Batteries. *Macromol. Rapid Commun.* **2024**, *45*, 2400184. [CrossRef]
69. Qiu, B.; Lin, B.; Yan, F. Ionic Liquid/Poly(Ionic Liquid)-Based Electrolytes for Energy Devices. *Polym. Int.* **2013**, *62*, 335–337. [CrossRef]
70. Tang, X.; Lv, S.; Jiang, K.; Zhou, G.; Liu, X. Recent Development of Ionic Liquid-Based Electrolytes in Lithium-Ion Batteries. *J. Power Sources* **2022**, *542*, 231792. [CrossRef]
71. Ahn, H.; Kim, D.; Lee, M.; Nam, K.W. Challenges and Possibilities for Aqueous Battery Systems. *Commun. Mater.* **2023**, *4*, 1–19. [CrossRef]
72. Yang, X.; Fan, H.; Hu, F.; Chen, S.; Yan, K.; Ma, L. Aqueous Zinc Batteries with Ultra-Fast Redox Kinetics and High Iodine Utilization Enabled by Iron Single Atom Catalysts. *Nano-Micro Lett.* **2023**, *15*, 126. [CrossRef]
73. Zhou, M.; Zhou, X.; Yang, Y.; Yin, H.; Lei, Y.; Liang, S.; Fang, G. Issues and Optimization Strategies of Binders for Aqueous Zinc Metal Batteries. *Chem. Eng. J.* **2024**, *497*, 154916. [CrossRef]
74. Li, L.; Jia, S.; Cheng, Z.; Zhang, C. Improved Strategies for Separators in Zinc-Ion Batteries. *ChemSusChem* **2023**, *16*, e202202330. [CrossRef] [PubMed]
75. Lu, M.; Yan, Y.; Zheng, Y.; Zhang, W.; He, X.; Wu, Z.; Yang, T.; Xia, X.; Huang, H.; Xia, Y.; et al. Recent Advances of Aqueous Rechargeable Lithium/Sodium Ion Batteries: Key Electrode Materials and Electrolyte Design Strategies. *Mater. Today Energy* **2023**, *38*, 101454. [CrossRef]

76. Lv, C.; Bao, L.; Huo, Y.; Liu, Y.; Su, Z. Enhancing the Hydrogen Ion Adsorption Capacity to Improve the Performance of an Aqueous Zinc Ion Battery of V<sub>2</sub>O<sub>5</sub>. *Inorg. Chem. Commun.* **2024**, *161*, 112053. [[CrossRef](#)]
77. Xie, J.; Lin, D.; Lei, H.; Wu, S.; Li, J.; Mai, W.; Wang, P.; Hong, G.; Zhang, W. Electrolyte and Interphase Engineering of Aqueous Batteries Beyond “Water-in-Salt” Strategy. *Adv. Mater.* **2024**, *36*, 2306508. [[CrossRef](#)]
78. Olana, B.N.; Pan, S.-H.; Hwang, B.-J.; Althues, H.; Jiang, J.-C.; Lin, S.D. Understanding the Formation Chemistry of Native Solid Electrolyte Interphase over Lithium Anode and Its Implications Using a LiTFSI/TME-TTE Electrolyte and Polysulfide Additive. *J. Mater. Chem. A* **2024**, *12*, 3659–3670. [[CrossRef](#)]
79. Jaumaux, P.; Yang, X.; Zhang, B.; Safaei, J.; Tang, X.; Zhou, D.; Wang, C.; Wang, G. Localized Water-In-Salt Electrolyte for Aqueous Lithium-Ion Batteries. *Angew. Chem. Int. Ed.* **2021**, *60*, 19965–19973. [[CrossRef](#)]
80. Suo, L.; Borodin, O.; Wang, Y.; Rong, X.; Sun, W.; Fan, X.; Xu, S.; Schroeder, M.A.; Cresce, A.V.; Wang, F.; et al. “Water-in-Salt” Electrolyte Makes Aqueous Sodium-Ion Battery Safe, Green, and Long-Lasting. *Adv. Energy Mater.* **2017**, *7*, 1701189. [[CrossRef](#)]
81. Nian, Q.; Zhu, W.; Zheng, S.; Chen, S.; Xiong, B.-Q.; Wang, Z.; Wu, X.; Tao, Z.; Ren, X. An Overcrowded Water-Ion Solvation Structure for a Robust Anode Interphase in Aqueous Lithium-Ion Batteries. *ACS Appl. Mater. Interfaces* **2021**, *13*, 51048–51056. [[CrossRef](#)]
82. Kumar, M.; Nagaiah, T.C. High Energy Density Aqueous Rechargeable Sodium-Ion/Sulfur Batteries in ‘water in Salt’ Electrolyte. *Energy Storage Mater.* **2022**, *49*, 390–400. [[CrossRef](#)]
83. Li, Y.; Xu, J.; Liu, H.; Hu, X.; Zhang, Q.; Peng, W.; Li, Y.; Zhang, F.; Han, Y.; Fan, X. Suppressing Vanadium Dissolution in “Water-in-Salt” Electrolytes for 3.2 V Aqueous Sodium-Ion Pseudocapacitors. *ACS Appl. Mater. Interfaces* **2022**, *14*, 35485–35494. [[CrossRef](#)]
84. Kumar, M.; Nagaiah, T.C. Tuning the Interfacial Chemistry for Stable and High Energy Density Aqueous Sodium-Ion/Sulfur Batteries. *J. Mater. Chem. A* **2022**, *10*, 12984–12996. [[CrossRef](#)]
85. Rao, R.; Chen, L.; Su, J.; Cai, S.; Wang, S.; Chen, Z. Issues and Challenges Facing Aqueous Sodium-ion Batteries toward Practical Applications. *Battery Energy* **2024**, *3*, 20230036. [[CrossRef](#)]
86. Droguet, L.; Grimaud, A.; Fontaine, O.; Tarascon, J. Water-in-Salt Electrolyte (WiSE) for Aqueous Batteries: A Long Way to Practicality. *Adv. Energy Mater.* **2020**, *10*, 2002440. [[CrossRef](#)]
87. Kühnel, R.-S.; Reber, D.; Remhof, A.; Figi, R.; Bleiner, D.; Battaglia, C. “Water-in-Salt” Electrolytes Enable the Use of Cost-Effective Aluminum Current Collectors for Aqueous High-Voltage Batteries. *Chem. Commun.* **2016**, *52*, 10435–10438. [[CrossRef](#)]
88. Kasprzak, D.; Wu, Z.; Tao, L.; Xu, J.; Zhang, Y.; Liu, J. Water-in-Salt Gel Biopolymer Electrolytes for Flexible and Wearable Zn/Alkali Metal Dual-Ion Batteries. *ACS Appl. Mater. Interfaces* **2024**, *16*, 36304–36314. [[CrossRef](#)] [[PubMed](#)]
89. Wang, Y.; Meng, X.; Sun, J.; Liu, Y.; Hou, L. Recent Progress in “Water-in-Salt” Electrolytes Toward Non-Lithium Based Rechargeable Batteries. *Front. Chem.* **2020**, *8*, 595. [[CrossRef](#)]
90. Sun, W.; Suo, L.; Wang, F.; Eidson, N.; Yang, C.; Han, F.; Ma, Z.; Gao, T.; Zhu, M.; Wang, C. “Water-in-Salt” Electrolyte Enabled LiMn<sub>2</sub>O<sub>4</sub>/TiS<sub>2</sub> Lithium-Ion Batteries. *Electrochem. Commun.* **2017**, *82*, 71–74. [[CrossRef](#)]
91. Yamada, Y.; Usui, K.; Sodeyama, K.; Ko, S.; Tateyama, Y.; Yamada, A. Hydrate-Melt Electrolytes for High-Energy-Density Aqueous Batteries. *Nat. Energy* **2016**, *1*, 16129. [[CrossRef](#)]
92. Ko, S.; Yamada, Y.; Miyazaki, K.; Shimada, T.; Watanabe, E.; Tateyama, Y.; Kamiya, T.; Honda, T.; Akikusa, J.; Yamada, A. Lithium-Salt Monohydrate Melt: A Stable Electrolyte for Aqueous Lithium-Ion Batteries. *Electrochem. Commun.* **2019**, *104*, 106488. [[CrossRef](#)]
93. Becker, M.; Kühnel, R.-S.; Battaglia, C. Water-in-Salt Electrolytes for Aqueous Lithium-Ion Batteries with Liquidus Temperatures below –10 °C. *Chem. Commun.* **2019**, *55*, 12032–12035. [[CrossRef](#)]
94. Wang, Y.; Ou, R.; Yang, J.; Xin, Y.; Singh, P.; Wu, F.; Qian, Y.; Gao, H. The Safety Aspect of Sodium Ion Batteries for Practical Applications. *J. Energy Chem.* **2024**, *95*, 407–427. [[CrossRef](#)]
95. Eshetu, G.G.; Grugeon, S.; Kim, H.; Jeong, S.; Wu, L.; Gachot, G.; Laruelle, S.; Armand, M.; Passerini, S. Comprehensive Insights into the Reactivity of Electrolytes Based on Sodium Ions. *ChemSusChem* **2016**, *9*, 462–471. [[CrossRef](#)] [[PubMed](#)]
96. Liu, T.; Yang, X.; Nai, J.; Wang, Y.; Liu, Y.; Liu, C.; Tao, X. Recent Development of Na Metal Anodes: Interphase Engineering Chemistries Determine the Electrochemical Performance. *Chem. Eng. J.* **2021**, *409*, 127943. [[CrossRef](#)]
97. Suo, L.; Oh, D.; Lin, Y.; Zhuo, Z.; Borodin, O.; Gao, T.; Wang, F.; Kushima, A.; Wang, Z.; Kim, H.-C.; et al. How Solid-Electrolyte Interphase Forms in Aqueous Electrolytes. *J. Am. Chem. Soc.* **2017**, *139*, 18670–18680. [[CrossRef](#)] [[PubMed](#)]
98. Kühnel, R.-S.; Reber, D.; Battaglia, C. A High-Voltage Aqueous Electrolyte for Sodium-Ion Batteries. *ACS Energy Lett.* **2017**, *2*, 2005–2006, Erratum in *ACS Energy Lett.* **2020**, *5*, 346. <https://doi.org/10.1021/acsenergylett.9b02779>. [[CrossRef](#)]
99. Han, J.; Zarabeitia, M.; Mariani, A.; Jusys, Z.; Hekmatfar, M.; Zhang, H.; Geiger, D.; Kaiser, U.; Behm, R.J.; Varzi, A.; et al. Halide-Free Water-in-Salt Electrolytes for Stable Aqueous Sodium-Ion Batteries. *Nano Energy* **2020**, *77*, 105176. [[CrossRef](#)]
100. Lee, M.H.; Kim, S.J.; Chang, D.; Kim, J.; Moon, S.; Oh, K.; Park, K.-Y.; Seong, W.M.; Park, H.; Kwon, G.; et al. Toward a Low-Cost High-Voltage Sodium Aqueous Rechargeable Battery. *Mater. Today* **2019**, *29*, 26–36. [[CrossRef](#)]

101. Jiang, L.; Liu, L.; Yue, J.; Zhang, Q.; Zhou, A.; Borodin, O.; Suo, L.; Li, H.; Chen, L.; Xu, K.; et al. High-Voltage Aqueous Na-Ion Battery Enabled by Inert-Cation-Assisted Water-in-Salt Electrolyte. *Adv. Mater.* **2020**, *32*, 1904427. [CrossRef] [PubMed]
102. Jin, T.; Ji, X.; Wang, P.; Zhu, K.; Zhang, J.; Cao, L.; Chen, L.; Cui, C.; Deng, T.; Liu, S.; et al. High-Energy Aqueous Sodium-Ion Batteries. *Angew. Chem. Int. Ed.* **2021**, *60*, 11943–11948. [CrossRef]
103. Han, J.; Mariani, A.; Zhang, H.; Zarzbeitia, M.; Gao, X.; Carvalho, D.V.; Varzi, A.; Passerini, S. Gelified Acetate-Based Water-in-Salt Electrolyte Stabilizing Hexacyanoferrate Cathode for Aqueous Potassium-Ion Batteries. *Energy Storage Mater.* **2020**, *30*, 196–205. [CrossRef]
104. Kumaresan, T.K.; Ikhe, A.B.; Park, W.; Prabakar, S.J.R.; Noh, H.S.; Seo, J.Y.; Lee, Y.; Sohn, K.; Kwak, J.S.; Pyo, M. Highly Concentrated Asymmetric KTFSI for Aqueous Potassium Ion Batteries. *Adv. Energy Mater.* **2024**, *14*, 2402011. [CrossRef]
105. Chen, N.; Gui, B.; Yang, B.; Deng, C.; Liang, Y.; Zhang, F.; Li, B.; Sun, W.; Wu, F.; Chen, R. LiPF<sub>6</sub> Induces Phosphorization of Garnet-Type Solid-State Electrolyte for Stable Lithium Metal Batteries. *Small* **2024**, *20*, 2305576. [CrossRef]
106. Chen, L.; Zhang, J.; Li, Q.; Vatamanu, J.; Ji, X.; Pollard, T.P.; Cui, C.; Hou, S.; Chen, J.; Yang, C.; et al. A 63 m Superconcentrated Aqueous Electrolyte for High-Energy Li-Ion Batteries. *ACS Energy Lett.* **2020**, *5*, 968–974. [CrossRef]
107. Akash Prabhu, S.; Kunhiraman, A.K.; Naveen, T.B.; Ajay Rakshesh, R.; Peeters, M. Recent Progress and Prospects in the Electrode Materials of Flexible Sodium-Ion Battery. *Sustain. Chem. Pharm.* **2022**, *28*, 100693. [CrossRef]
108. Ye, C.; Zhang, L.; Guo, C.; Li, D.; Vasileff, A.; Wang, H.; Qiao, S. A 3D Hybrid of Chemically Coupled Nickel Sulfide and Hollow Carbon Spheres for High Performance Lithium–Sulfur Batteries. *Adv. Funct. Mater.* **2017**, *27*, 1702524. [CrossRef]
109. Simanjuntak, E.K.; Danner, T.; Wang, P.; Buchmeiser, M.R.; Latz, A. A Novel Modeling Approach for Sulfurized Polyacrylonitrile (SPAN) Electrodes in Li Metal Batteries. *Electrochim. Acta* **2024**, *497*, 144571. [CrossRef]
110. Han, J.; Zhang, H.; Varzi, A.; Passerini, S. Fluorine-Free Water-in-Salt Electrolyte for Green and Low-Cost Aqueous Sodium-Ion Batteries. *ChemSusChem* **2018**, *11*, 3704–3707. [CrossRef]
111. Qiu, S.; Xu, Y.; Wu, X.; Ji, X. Prussian Blue Analogues as Electrodes for Aqueous Monovalent Ion Batteries. *Electrochem. Energy Rev.* **2022**, *5*, 242–262. [CrossRef]
112. Ahaliabadeh, Z.; Miikkulainen, V.; Mäntymäki, M.; Colalongo, M.; Mousavihashemi, S.; Yao, L.; Jiang, H.; Lahtinen, J.; Kankaanpää, T.; Kallio, T. Stabilized Nickel-Rich-Layered Oxide Electrodes for High-Performance Lithium-Ion Batteries. *Energy Environ. Mater.* **2024**, *7*, e12741. [CrossRef]
113. Cui, M.; Liu, M.; Li, X.; Shi, W.; Yu, Y.; Li, J.; Liu, Y.; Zhang, F.; Wang, W.; Li, X.; et al. Order-Disorder Structural Engineering of Vanadium Oxide Anode: Balancing Ionic and Electronic Dynamic for Fast-Charging Aqueous Li-Ion Battery. *Energy Storage Mater.* **2024**, *70*, 103453. [CrossRef]
114. Kim, M.; Lee, S.; Kang, B. High Energy Density Polyanion Electrode Material: LiVPO<sub>4</sub>O<sub>1-x</sub>F<sub>x</sub> ( $x \approx 0.25$ ) with Tavorite Structure. *Chem. Mater.* **2017**, *29*, 4690–4699. [CrossRef]
115. Sun, X.; Tripathi, R.; Popov, G.; Balasubramanian, M.; Nazar, L.F. Stabilization of Lithium Transition Metal Silicates in the Olivine Structure. *Inorg. Chem.* **2017**, *56*, 9931–9937. [CrossRef]
116. Cambaz, M.A.; Anji Reddy, M.; Vinayan, B.P.; Witte, R.; Pohl, A.; Mu, X.; Chakravadhanula, V.S.K.; Kübel, C.; Fichtner, M. Mechanical Milling Assisted Synthesis and Electrochemical Performance of High Capacity LiFeBO<sub>3</sub> for Lithium Batteries. *ACS Appl. Mater. Interfaces* **2016**, *8*, 2166–2172. [CrossRef] [PubMed]
117. Wang, Q.; Wu, X.; You, H.; Min, H.; Xu, X.; Hao, J.; Liu, X.; Yang, H. Template-Directed Prussian Blue Nanocubes Supported on Ni Foam as the Binder-Free Anode of Lithium-Ion Batteries. *Appl. Surf. Sci.* **2022**, *571*, 151194. [CrossRef]
118. Zhang, Z.; Avdeev, M.; Chen, H.; Yin, W.; Kan, W.H.; He, G. Lithiated Prussian Blue Analogues as Positive Electrode Active Materials for Stable Non-Aqueous Lithium-Ion Batteries. *Nat. Commun.* **2022**, *13*, 7790. [CrossRef]
119. Wi, T.-U.; Park, C.; Ko, S.; Kim, T.; Choi, A.; Muralidharan, V.; Choi, M.; Lee, H.-W. Cathode Electrolyte Interphase Engineering for Prussian Blue Analogues in Lithium-Ion Batteries. *Nano Lett.* **2024**, *24*, 7783–7791. [CrossRef]
120. Yang, C.; Chen, J.; Qing, T.; Fan, X.; Sun, W.; Von Cresce, A.; Ding, M.S.; Borodin, O.; Vatamanu, J.; Schroeder, M.A.; et al. 4.0 V Aqueous Li-Ion Batteries. *Joule* **2017**, *1*, 122–132. [CrossRef]
121. He, Z.; Huang, Y.; Liu, H.; Geng, Z.; Li, Y.; Li, S.; Deng, W.; Zou, G.; Hou, H.; Ji, X. Anode Materials for Fast Charging Sodium-Ion Batteries. *Nano Energy* **2024**, *129*, 109996. [CrossRef]
122. Maddukuri, S.; Nimkar, A.; Chae, M.S.; Penki, T.R.; Luski, S.; Aurbach, D. Na<sub>0.44</sub>MnO<sub>2</sub>/Polyimide Aqueous Na-Ion Batteries for Large Energy Storage Applications. *Front. Energy Res.* **2021**, *8*, 615677. [CrossRef]
123. Kumaresan, L.; Kirubakaran, K.P.; Priyadarshini, M.; Kasiviswanathan, K.; Senthil, C.; Lee, C.W.; Vediappan, K. Sustainable-Inspired Design of Efficient Organic Electrodes for Rechargeable Sodium-Ion Batteries: Conversion of P-Waste into E-Wealth Device. *Sustain. Mater. Technol.* **2021**, *28*, e00247. [CrossRef]
124. Zhang, H.; Jeong, S.; Qin, B.; Vieira Carvalho, D.; Buchholz, D.; Passerini, S. Towards High-Performance Aqueous Sodium-Ion Batteries: Stabilizing the Solid/Liquid Interface for NASICON-Type Na<sub>2</sub> VTi(PO<sub>4</sub>)<sub>3</sub> Using Concentrated Electrolytes. *ChemSusChem* **2018**, *11*, 1382–1389. [CrossRef] [PubMed]

125. Nakamoto, K.; Sakamoto, R.; Nishimura, Y.; Xia, J.; Ito, M.; Okada, S. A Trifluoroacetate-Based Concentrated Electrolyte for Symmetrical Aqueous Sodium-Ion Battery with NASICON-Type  $\text{Na}_2\text{VTi}(\text{PO}_4)_3$  Electrodes. *Electrochemistry* **2021**, *89*, 415–419. [[CrossRef](#)]
126. Suo, L.; Han, F.; Fan, X.; Liu, H.; Xu, K.; Wang, C. “Water-in-Salt” Electrolytes Enable Green and Safe Li-Ion Batteries for Large Scale Electric Energy Storage Applications. *J. Mater. Chem. A* **2016**, *4*, 6639–6644. [[CrossRef](#)]
127. Wang, F.; Suo, L.; Liang, Y.; Yang, C.; Han, F.; Gao, T.; Sun, W.; Wang, C. Spinel  $\text{LiNi}_{0.5}\text{Mn}_{1.5}\text{O}_4$  Cathode for High-Energy Aqueous Lithium-Ion Batteries. *Adv. Energy Mater.* **2017**, *7*, 1600922. [[CrossRef](#)]
128. Liang, G.; Gan, Z.; Wang, X.; Jin, X.; Xiong, B.; Zhang, X.; Chen, S.; Wang, Y.; He, H.; Zhi, C. Reconstructing Vanadium Oxide with Anisotropic Pathways for a Durable and Fast Aqueous K-Ion Battery. *ACS Nano* **2021**, *15*, 17717–17728. [[CrossRef](#)]
129. Luo, W.; Hayden, J.; Jang, S.-H.; Wang, Y.; Zhang, Y.; Kuang, Y.; Wang, Y.; Zhou, Y.; Rubloff, G.W.; Lin, C.-F.; et al. Highly Conductive, Light Weight, Robust, Corrosion-Resistant, Scalable, All-Fiber Based Current Collectors for Aqueous Acidic Batteries. *Adv. Energy Mater.* **2018**, *8*, 1702615. [[CrossRef](#)]
130. Levi, N.; Bergman, G.; Nimkar, A.; Tsubery, M.N.; Borenstein, A.; Adronov, A.; Aurbach, D.; Sharon, D.; Nessim, G.D.; Shpigel, N. Carbon Nanotubes as Efficient Anode Current Collectors for Stationary Aqueous Zn–Br<sub>2</sub> Batteries. *Carbon* **2024**, *228*, 119407. [[CrossRef](#)]
131. Li, S.; Church, B.C. Electrochemical Stability of Aluminum Current Collector in Aqueous Rechargeable Lithium-Ion Battery Electrolytes. *J. Appl. Electrochem.* **2017**, *47*, 839–853. [[CrossRef](#)]
132. Hou, Z.; Zhang, X.; Ao, H.; Liu, M.; Zhu, Y.; Qian, Y. Passivation Effect for Current Collectors Enables High-Voltage Aqueous Sodium Ion Batteries. *Mater. Today Energy* **2019**, *14*, 100337. [[CrossRef](#)]
133. Wen, Y.H.; Shao, L.; Zhao, P.C.; Wang, B.Y.; Cao, G.P.; Yang, Y.S. Carbon Coated Stainless Steel Mesh as a Low-Cost and Corrosion-Resistant Current Collector for Aqueous Rechargeable Batteries. *J. Mater. Chem. A* **2017**, *5*, 15752–15758. [[CrossRef](#)]
134. Ren, H.; Zhang, X.; Liu, Q.; Tang, W.; Liang, J.; Wu, W. Fully-Printed Flexible Aqueous Rechargeable Sodium-Ion Batteries. *Small* **2024**, *20*, 2312207. [[CrossRef](#)]
135. Kucinskis, G.; Kruze, B.; Korde, P.; Sarakovskis, A.; Viksna, A.; Hodakovska, J.; Bajars, G. Enhanced Electrochemical Properties of  $\text{Na}_0.67\text{MnO}_2$  Cathode for Na-Ion Batteries Prepared with Novel Tetrabutylammonium Alginate Binder. *Batteries* **2022**, *8*, 6. [[CrossRef](#)]
136. Pace, G.T.; Wang, H.; Whitacre, J.F.; Wu, W. Comparative Study of Water-Processable Polymeric Binders in  $\text{LiMn}_2\text{O}_4$  Cathode for Aqueous Electrolyte Batteries. *Nano Sel.* **2021**, *2*, 939–947. [[CrossRef](#)]
137. Malchik, F.; Shpigel, N.; Levi, M.D.; Penki, T.R.; Gavriel, B.; Bergman, G.; Turgeman, M.; Aurbach, D.; Gogotsi, Y. MXene Conductive Binder for Improving Performance of Sodium-Ion Anodes in Water-in-Salt Electrolyte. *Nano Energy* **2021**, *79*, 105433. [[CrossRef](#)]
138. Chen, B.; Zhang, Z.; Xiao, M.; Wang, S.; Huang, S.; Han, D.; Meng, Y. Polymeric Binders Used in Lithium Ion Batteries: Actualities, Strategies and Trends. *ChemElectroChem* **2024**, *11*, e202300651. [[CrossRef](#)]
139. Yi, H.; Lan, T.; Yang, Y.; Zeng, H.; Zhang, T.; Tang, T.; Wang, C.; Deng, Y. A Robust Aqueous-Processable Polymer Binder for Long-Life, High-Performance Lithium Sulfur Battery. *Energy Storage Mater.* **2019**, *21*, 61–68. [[CrossRef](#)]
140. Ao, H.; Chen, C.; Hou, Z.; Cai, W.; Liu, M.; Jin, Y.; Zhang, X.; Zhu, Y.; Qian, Y. Electrolyte Solvation Structure Manipulation Enables Safe and Stable Aqueous Sodium Ion Batteries. *J. Mater. Chem. A* **2020**, *8*, 14190–14197. [[CrossRef](#)]
141. He, B.; Man, P.; Zhang, Q.; Fu, H.; Zhou, Z.; Li, C.; Li, Q.; Wei, L.; Yao, Y. All Binder-Free Electrodes for High-Performance Wearable Aqueous Rechargeable Sodium-Ion Batteries. *Nano-Micro Lett.* **2019**, *11*, 101. [[CrossRef](#)]
142. Kang, Y.; Deng, C.; Chen, Y.; Liu, X.; Liang, Z.; Li, T.; Hu, Q.; Zhao, Y. Binder-Free Electrodes and Their Application for Li-Ion Batteries. *Nanoscale Res. Lett.* **2020**, *15*, 112. [[CrossRef](#)]
143. Liu, W.; Liu, W.; Jiang, Y.; Gui, Q.; Ba, D.; Li, Y.; Liu, J. Binder-Free Electrodes for Advanced Potassium-Ion Batteries: A Review. *Chin. Chem. Lett.* **2021**, *32*, 1299–1308. [[CrossRef](#)]
144. Arora, P.; Zhang, Z. Battery Separators. *Chem. Rev.* **2004**, *104*, 4419–4462. [[CrossRef](#)] [[PubMed](#)]
145. Yuan, B.; Wen, K.; Chen, D.; Liu, Y.; Dong, Y.; Feng, C.; Han, Y.; Han, J.; Zhang, Y.; Xia, C.; et al. Composite Separators for Robust High Rate Lithium Ion Batteries. *Adv. Funct. Mater.* **2021**, *31*, 2101420. [[CrossRef](#)]
146. Lee, H.; Yanilmaz, M.; Toprakci, O.; Fu, K.; Zhang, X. A Review of Recent Developments in Membrane Separators for Rechargeable Lithium-Ion Batteries. *Energy Environ. Sci.* **2014**, *7*, 3857–3886. [[CrossRef](#)]
147. Li, Y.; Yu, L.; Hu, W.; Hu, X. Thermotolerant Separators for Safe Lithium-Ion Batteries under Extreme Conditions. *J. Mater. Chem. A* **2020**, *8*, 20294–20317. [[CrossRef](#)]
148. Deerattrakul, V.; Sakulaue, P.; Bunpheng, A.; Kraithong, W.; Pengsawang, A.; Chakthranont, P.; Iamprasertkun, P.; Itthibenchapong, V. Introducing Hydrophilic Cellulose Nanofiber as a Bio-Separator for “Water-in-Salt” Based Energy Storage Devices. *Electrochim. Acta* **2023**, *453*, 142355. [[CrossRef](#)]
149. Peled, E. The Electrochemical Behavior of Alkali and Alkaline Earth Metals in Nonaqueous Battery Systems—The Solid Electrolyte Interphase Model. *J. Electrochem. Soc.* **1979**, *126*, 2047. [[CrossRef](#)]

150. Yue, J.; Lin, L.; Jiang, L.; Zhang, Q.; Tong, Y.; Suo, L.; Hu, Y.; Li, H.; Huang, X.; Chen, L. Interface Concentrated-Confinement Suppressing Cathode Dissolution in Water-in-Salt Electrolyte. *Adv. Energy Mater.* **2020**, *10*, 2000665. [[CrossRef](#)]
151. Cheng, X.; Zhang, R.; Zhao, C.; Wei, F.; Zhang, J.; Zhang, Q. A Review of Solid Electrolyte Interphases on Lithium Metal Anode. *Adv. Sci.* **2016**, *3*, 1500213. [[CrossRef](#)]
152. Mense, M.; Bela, M.M.; Kühn, S.P.; Cekic-Laskovic, I.; Börner, M.; Wiemers-Meyer, S.; Winter, M.; Nowak, S. ToF-SIMS Sputter Depth Profiling of Interphases and Coatings on Lithium Metal Surfaces. *Commun. Chem.* **2025**, *8*, 31. [[CrossRef](#)]
153. Sakamoto, R.; Yamashita, M.; Nakamoto, K.; Zhou, Y.; Yoshimoto, N.; Fujii, K.; Yamaguchi, T.; Kitajou, A.; Okada, S. Local Structure of a Highly Concentrated NaClO<sub>4</sub> Aqueous Solution-Type Electrolyte for Sodium Ion Batteries. *Phys. Chem. Chem. Phys.* **2020**, *22*, 26452–26458. [[CrossRef](#)]
154. Lazarenko, V.; Rublova, Y.; Meija, R.; Andzane, J.; Voikiva, V.; Kons, A.; Sarakovskis, A.; Viksna, A.; Erts, D. Bi<sub>2</sub>Se<sub>3</sub> Nanostructured Thin Films as Perspective Anodes for Aqueous Rechargeable Lithium-Ion Batteries. *Batteries* **2022**, *8*, 144. [[CrossRef](#)]
155. Zhang, J.; Cui, C.; Wang, P.-F.; Li, Q.; Chen, L.; Han, F.; Jin, T.; Liu, S.; Choudhary, H.; Raghavan, S.R.; et al. “Water-in-Salt” Polymer Electrolyte for Li-Ion Batteries. *Energy Environ. Sci.* **2020**, *13*, 2878–2887. [[CrossRef](#)]
156. Li, Y.; Zhou, Z.; Deng, W.; Li, C.; Yuan, X.; Hu, J.; Zhang, M.; Chen, H.; Li, R. A Superconcentrated Water-in-Salt Hydrogel Electrolyte for High-Voltage Aqueous Potassium-Ion Batteries. *ChemElectroChem* **2021**, *8*, 1451–1454. [[CrossRef](#)]

**Disclaimer/Publisher’s Note:** The statements, opinions and data contained in all publications are solely those of the individual author(s) and contributor(s) and not of MDPI and/or the editor(s). MDPI and/or the editor(s) disclaim responsibility for any injury to people or property resulting from any ideas, methods, instructions or products referred to in the content.